THE GEOLOGICAL SOCIETY OF AMERICA®

Accuracy and precision of the late Eocene–early Oligocene geomagnetic polarity time scale

Diana Sahy[1,2,†], Joe Hiess[1], Anne U. Fischer[3], Daniel J. Condon[1], Dennis O. Terry, Jr.[4], Hemmo A. Abels[5], Silja K. Hüsing[5], and Klaudia F. Kuiper[3,5]

[1]*NERC Isotope Geosciences Laboratory, British Geological Survey, Keyworth, NG12 5GG, UK*
[2]*Department of Geology, University of Leicester, University Road, Leicester, LE1 7RH, UK*
[3]*Faculty of Earth and Life Sciences, Vrije Universiteit, 1085 De Boelelaan, Amsterdam, 1081 HV, The Netherlands*
[4]*Department of Earth and Environmental Science, Temple University, Philadelphia, Pennsylvania 19122, USA*
[5]*Department of Earth Sciences, Utrecht University, Budapestlaan 17, 3584 CD, The Netherlands*

ABSTRACT

An accurate and precise geomagnetic polarity time scale is crucial to the development of a chronologic framework in which to test paleoclimatic and paleoenvironmental interpretations of marine and terrestrial records of the Eocene–Oligocene transition (EOT). The magnetic polarity patterns of relatively continuous marine and terrestrial records of the EOT have been dated using both radioisotopic techniques and astronomical tuning, both of which can achieve a precision approaching ±30 k.y. for much of the Paleogene. However, the age of magnetic reversals between chrons C12n and C16n.2n has proved difficult to calibrate, with discrepancies of up to 250 k.y. between radio-isotopically dated and astronomically tuned marine successions, rising to 600 k.y. for comparisons with the $^{206}Pb/^{238}U$-dated terrestrial record of the White River Group in North America. In this study, we reevaluate the magnetic polarity pattern of the Flagstaff Rim and Toadstool Geologic Park records of the White River Group (C12n–C16n.2n). Our interpretation of the Flagstaff Rim polarity record differs significantly from earlier studies, identifying a previously unreported normal polarity zone correlated to C15n, which eliminates discrepancies between the WRG and the $^{206}Pb/^{238}U$-dated marine record of the Rupelian Global Stratotype Section and Point in the Italian Umbria-Marche basin. However, residual discrepancies persist between U-Pb–dated and astronomically tuned records of the EOT even when stratigraphic and systematic uncertainties associated with each locality and dating method are taken into account, which suggests that the uncertainties associated with astronomically tuned records of the EOT may have been underestimated.

1. INTRODUCTION

Sedimentary records of the abrupt greenhouse–icehouse shift that marks the Eocene–Oligocene transition (EOT) are abundant both on continental landmasses and in the world's oceans. However, dating these records in order to assess global climate dynamics across the EOT can be problematic. Deepening of the carbonate compensation depth during this time limited the availability of carbonate-rich marine sediments (Coxall et al., 2005; Merico et al., 2008), while a base-level drop associated with the inception of the Antarctic ice sheet caused gaps in terrestrial sedimentary archives, particularly in coastal areas (Ivany et al., 2006; Shackleton and Kennett, 1975; Zachos et al., 2001). As a result, most records of the EOT are unsuitable for astronomical tuning. Additionally, the limited availability of volcanic ash beds hampers radio-isotopic dating based on the $^{40}Ar/^{39}Ar$ and $^{206}Pb/^{238}U$ systems.

Relative dating of EOT records based on correlating local magnetic polarity patterns to the Paleogene geomagnetic polarity time scale (GPTS) provides a solution to this problem. However, calibrating the late Eocene–early Oligocene portion of the GPTS is not straightforward. The most recent versions of the conventional Paleogene GPTS have relied on cubic spline interpolation along a synthetic South Atlantic marine magnetic anomaly profile (e.g., Cande and Kent, 1992) under the assumption of smoothly varying seafloor spreading rates (Cande and Kent, 1995; Berggren et al., 1985; Ogg and Smith, 2004; Vandenberghe et al., 2012). The spline curve was anchored by radioisotopically or astronomically dated tie-points from well-calibrated magnetostratigraphic records. However, recent $^{206}Pb/^{238}U$ dating of volcanic ash layers from the Umbria-Marche basin (UMB) sedimentary succession in central Italy has demonstrated that late Eocene and Oligocene $^{40}Ar/^{39}Ar$ dates used as tie-points in all recent GPTS compilations are anomalously old by ca. 400 k.y. (Sahy et al. 2017). Furthermore, the uncertainties associated with magnetic reversal ages between 31 and 36 Ma are around ± 0.2–0.5 m.y. in the most recent, 2012 edition of the geological time scale (Vandenberghe et al., 2012). (Unless otherwise stated, all uncertainties in this study are quoted at the 2σ level.) Precision will likely improve with the addition of further tie-points, but is currently almost one order of magnitude higher than that achievable by state-of-the art astronomical tuning and radio-isotopic dating methods (e.g., Hinnov and Ogg, 2007; Schoene et al., 2013). Consequently, the usefulness of magnetostratigraphic dating is limited when applied to records of comparatively rapid environmental change.

Some of the difficulties inherent to the radioisotopically calibrated GPTS can be circumvented by compiling magnetostratigraphic data from astronomically tuned deep marine records spanning several m.y., thereby eliminating the uncertainties related to interpolation between widely spaced tie-points and potential variability in seafloor spreading rates. Considerable effort has been directed toward achieving complete coverage of the Paleogene using this technique (Hilgen et al., 2010; Pälike et al., 2006; Westerhold and Röhl, 2009; Westerhold et al., 2007, 2008, 2011). The accuracy of astronomically

[†]dihy@bgs.ac.uk

GSA Bulletin; January/February 2020; v. 132; no. 1/2; p. 373–388; https://doi.org/10.1130/B35184.1; 9 figures; 2 tables; Data Repository item 2019238; published online 13 June 2019.

tuned age models is underpinned by numerical models of insolation (e.g., Laskar et al., 2004, 2011), but ultimately depends upon the complete expression and accurate identification of eccentricity, and where appropriate, obliquity and precession cycles in the sedimentary record. The validity of the tuning can be further tested by evaluating hierarchical cycle patterns, i.e., the presence of cycles whose durations conform to the 1:2:5:20 ratio expected for precession (21 k.y.), obliquity (40 k.y.), and eccentricity (100 and 405 k.y.), and identifying amplitude or frequency modulations that are calculated based on theoretical precession and obliquity signals (e.g., Meyers, 2015). Astronomically tuned time scales have been developed for the Oligocene (Pälike et al., 2006) the Paleocene (Kuiper et al., 2008; Westerhold et al., 2008; Dinares-Turell et al., 2014; Hilgen et al., 2015), and much of the Eocene (Pälike et al., 2001; Westerhold and Röhl, 2009; Westerhold et al., 2014). However, the tuning of the EOT interval has proven to be problematic due to the scarcity of suitable carbonate-rich deep marine records, resulting in a late Eocene "gap" between 33.7 and 47.8 Ma in the astronomically tuned GPTS of the geological time scale. This gap has recently been closed (Westerhold et al., 2015; Boulila et al., 2018) but the entire Eocene–Oligocene part of the astronomical time scale still requires independent confirmation and testing by state-of-the-art radio-isotopic dating. Two of the above astronomically tuned records are relevant to the present study, namely those from ODP Site 1218 (ATPS06, Pälike et al., 2006), and the Pacific Equatorial Age Transect (PEAT, Westerhold et al. 2014) (Fig. 1). Between chrons C12n and C16n.2n, the discrepancies in nominal magnetic reversal age between these two records are ~0.2–0.25 m.y. (Fig. 1). Data on the precision of the tuning of the PEAT and ATPS06 records are not reported in the literature, although Westerhold et al. (2014) do quote uncertainties associated with the stratigraphic placement of magnetic reversal for the former, which range between 4 and 44 k.y. for this interval. If we assume a conservative tuning uncertainty of ± 50 k.y. (i.e., half of one 100 k.y. eccentricity cycle) for both the ATPS06 and PEAT records, the discrepancies between the two appear to be statistically significant at the 95% confidence level (Fig. 1).

The validity of astronomically tuned time scales of the EOT may be tested through comparisons with radio-isotopically dated volcanic tuffs from magnetostratigraphically calibrated land-based sections. Two such records, dated using the $^{206}Pb/^{238}U$ isotope system in zircon, are available from the UMB in central Italy (Sahy et al., 2017) and the White River Group (WRG) in central North America (Sahy et al., 2015) (Fig. 1). The accuracy of $^{206}Pb/^{238}U$ dating is underpinned by gravimetrically calibrated isotopic tracer solutions developed through the community-driven EARTHTIME initiative (Condon et al., 2015; McLean et al., 2015), and the ^{238}U decay constant (Jaffey et al., 1971). $^{206}Pb/^{238}U$ dating is capable of producing results with a precision of ~0.10–0.15%, or ~40–60 k.y. for a sample around 34 Ma in age. This includes systematic uncertainties associated with isotopic tracer calibration and the ^{238}U decay constant, which must be propagated in order to compare U-Pb results with data from other dating methods. Although the precision of interpolated age depth models developed for these records is somewhat lower than that of individual $^{206}Pb/^{238}U$ dates, magnetic reversal between C12n and C16n.2n can be constrained to ±40–150 k.y. in both the UMB and WRG records.

A comparison between magnetic reversal ages derived from the ATPS06, PEAT, UMB and WRG records reveals discrepancies of up to a few hundred k.y. both between records calibrated using the same dating method, and between records dated using astronomical tuning and the $^{206}Pb/^{238}U$ isotope system. The largest discrepancies are observed relative to the WRG record (Fig. 1), whose magnetic polarity pattern (Prothero et al., 1983; Prothero and Swisher, 1992) is constrained by the $^{206}Pb/^{238}U$ dates of Sahy et al. (2015). The aim of this paper is to reevaluate the magnetic polarity pattern of the Flagstaff Rim (FR, central Wyoming) and Toadstool Geologic Park (TGP, NE Nebraska) localities from which the $^{206}Pb/^{238}U$ dates calibrating the WRG are sourced. We then assess the strengths and weaknesses of different records and dating methods in order to refine the calibration of the GPTS across the EOT.

2. GEOLOGICAL SETTING AND PUBLISHED MAGNETOSTRATIGRAPHY OF THE WHITE RIVER GROUP

The WRG encompasses fluvial, eolian, and minor lacustrine deposits that accumulated on the North American mid-continent during the late Eocene–Oligocene (ca. 37–29 Ma) and can be traced laterally from North Dakota into NW Nebraska, E Wyoming, and NE Colorado (Fig. 2). Hosting some of the richest Paleogene mammal fossil assemblages in the world, the WRG forms the basis for the definition of the Chadronian (late Eocene), Orellan, and Whitneyan (early Oligocene) North American Land Mammal Ages (NALMAs).

The bulk of the WRG consists of fine-grained, reworked volcaniclastic material, with subordinate siliciclastic input derived from the Hartville, Laramie, and Black Hills uplifts (Clark, 1975; Stanley and Benson, 1979). The source of the reworked volcaniclastic material was explosive volcanism in present-day Utah and Nevada (Larson and Evanoff, 1998), ~500–800 km SW of the main WRG outcrops, which also produced numerous primary air-fall tuffs that are intercalated in the WRG record. Consequently, the thickness of individual stratigraphic units, and the grainsize of primary air-fall tuffs decreases from SW to NE, as distance from the source area increases (Emry et al., 1987). Lithostratigraphic nomenclature varies between localities with White River deposits ranked as a group in Nebraska and South Dakota and as a formation in Wyoming (LaGarry, 1998; Terry, 1998; Terry and LaGarry, 1998). The paleontologic and paleoclimatologic significance of the WRG record prompted extensive magnetostratigraphic (Prothero et al., 1982; Prothero 1985, 1996; Prothero and Swisher 1992) and geochronologic investigations (Evernden et al., 1964; Swisher and Prothero, 1990; Obradovich et al., 1995; Terry, 2001; Zanazzi et al., 2007, 2009; Boardman and Secord, 2013; Sahy et al., 2015), aimed at elucidating the rate of faunal and environmental change across the Chadronian–Whitneyan NALMAs and its relationship to the marine record of the EOT. Samples for the current study were collected from Flagstaff Rim (FR) in central Wyoming, and Toadstool Geologic Park (TGP) in NW Nebraska, with the aim of reevaluating the magnetic polarity patterns recorded at these localities.

2.1. Flagstaff Rim

The FR section, ~20 km SW of Casper in central Wyoming (Fig. 2A), consists of a 200-m-high cliff and smaller surrounding outcrops of volcaniclastic overbank siltstones, interbedded with tabular and lenticular channel sandstones belonging to the White River Formation. The White River Formation unconformably overlies the Cretaceous Cody Shale and is in turn unconformably overlain by the Miocene Split Rock Formation (Emry, 1973). Seventeen volcanic tuffs have been identified at Flagstaff Rim (Fig. 2B), the most prominent of which are labeled A to J (Emry, 1973). The entire FR record is of Chadronian (late Eocene) age (Emry, 1992), with the type section for the Middle Chadronian starting 15 m below the B tuff and ending 15 m above the G tuff (Prothero, 1996). The interval between the B and J tuffs spans 1.4 m.y. (Sahy et al., 2015).

The current interpretation of the magnetic polarity pattern of the FR section includes two normal polarity zones (Prothero et al., 1982, 1983),

the extent of which has been revised by Prothero (1985) and Prothero and Swisher (1992). The two normal polarity zones were correlated to C15n and C16n.1n based on late Eocene biotite and anorthoclase $^{40}Ar/^{39}Ar$ dates from tuffs B, F, G, I, and J (Swisher and Prothero, 1990). However, subsequent $^{40}Ar/^{39}Ar$ dating of sanidines from the B and J tuffs (Obradovich et al., 1995), and more extensive $^{206}Pb/^{238}U$ dating of zircons from nine of the FR tuffs (including B and J) cast doubts on the validity of these correlations, as the $^{40}Ar/^{39}Ar$ dates of Swisher and Prothero (1990) were found to be anomalously old by up to 1 m.y., probably due to the presence of detrital anorthoclase and biotite grains among the analyzed fractions (Sahy et al., 2015).

2.2. Toadstool Geologic Park

Toadstool Geologic Park (TGP), ~20 km W of Chadron in NW Nebraska (Fig. 2A), consists of a series of laterally continuous outcrops covering ca. 6 km^2 along Big Cottonwood Creek. Lithostratigraphically, the TGP succession comprises the Chadron and Brule Formations of the WRG (Fig. 2C). The Chadron Formation is further subdivided into the Peanut Peak Member, consisting of bluish green, gray, and olive claystones (Terry, 1998), and the overlying Big Cottonwood Creek Member which comprises primarily volcaniclastic overbank silty claystones, interbedded with tabular and lenticular channel sandstones (Terry and LaGarry, 1998). The

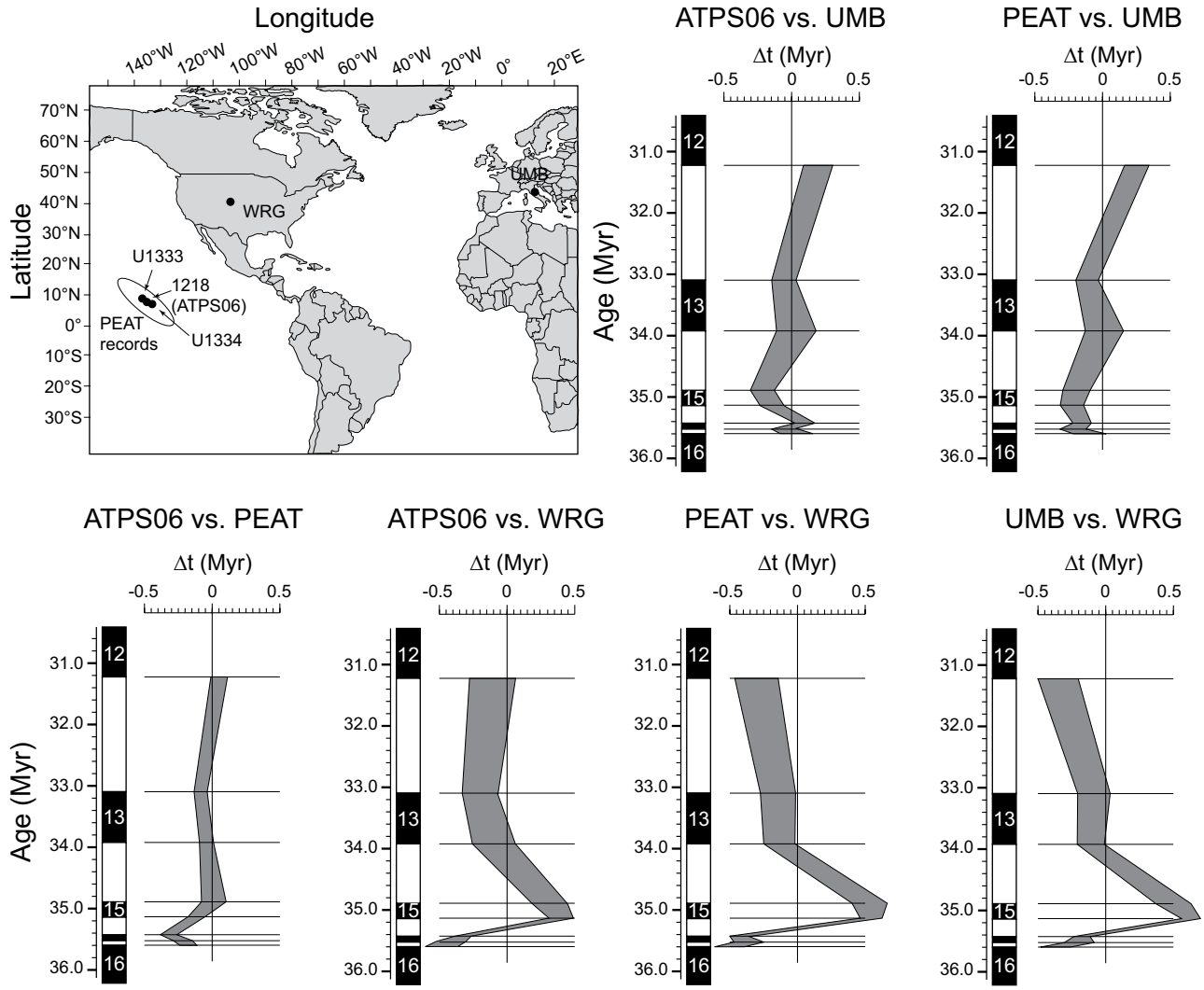

Figure 1. Comparison between astronomically tuned and U-Pb calibrated time scales of the late Eocene and early Oligocene. ATPS06—tuning of ODP Site 1218 (Pälike et al., 2006), PEAT—tuning of the Pacific Equatorial Age Transect (Westerhold et al., 2014) based on sites 1218, U1333, and U1334. WRG—magnetostratigraphy of the White River Group based on $^{206}Pb/^{238}U$ dating of volcanic tuffs from Flagstaff Rim and Toadstool Geologic Park (Sahy et al., 2015) and the magnetic polarity patterns of Prothero (1985) for Flagstaff Rim, and Prothero et al. (1983) for TGP. UMB—magnetostratigraphy of the Umbria-Marche basin based on $^{206}Pb/^{238}U$ dating of volcanic ash beds from Massignano and Monte Cagnero (Sahy et al., 2017) and the magnetic polarity patterns of Jovane et al. (2006) and Lowrie and Lanci (1994) for Massignano, and Hyland et al. (2009) and Jovane et al. (2013) for Monte Cagnero. Uncertainties were propagated based on Equations S1–S6 in Section S2 of the Supplementary Material (see footnote 1). Note that for the purpose of this figure, stratigraphic uncertainties are assumed to be zero.

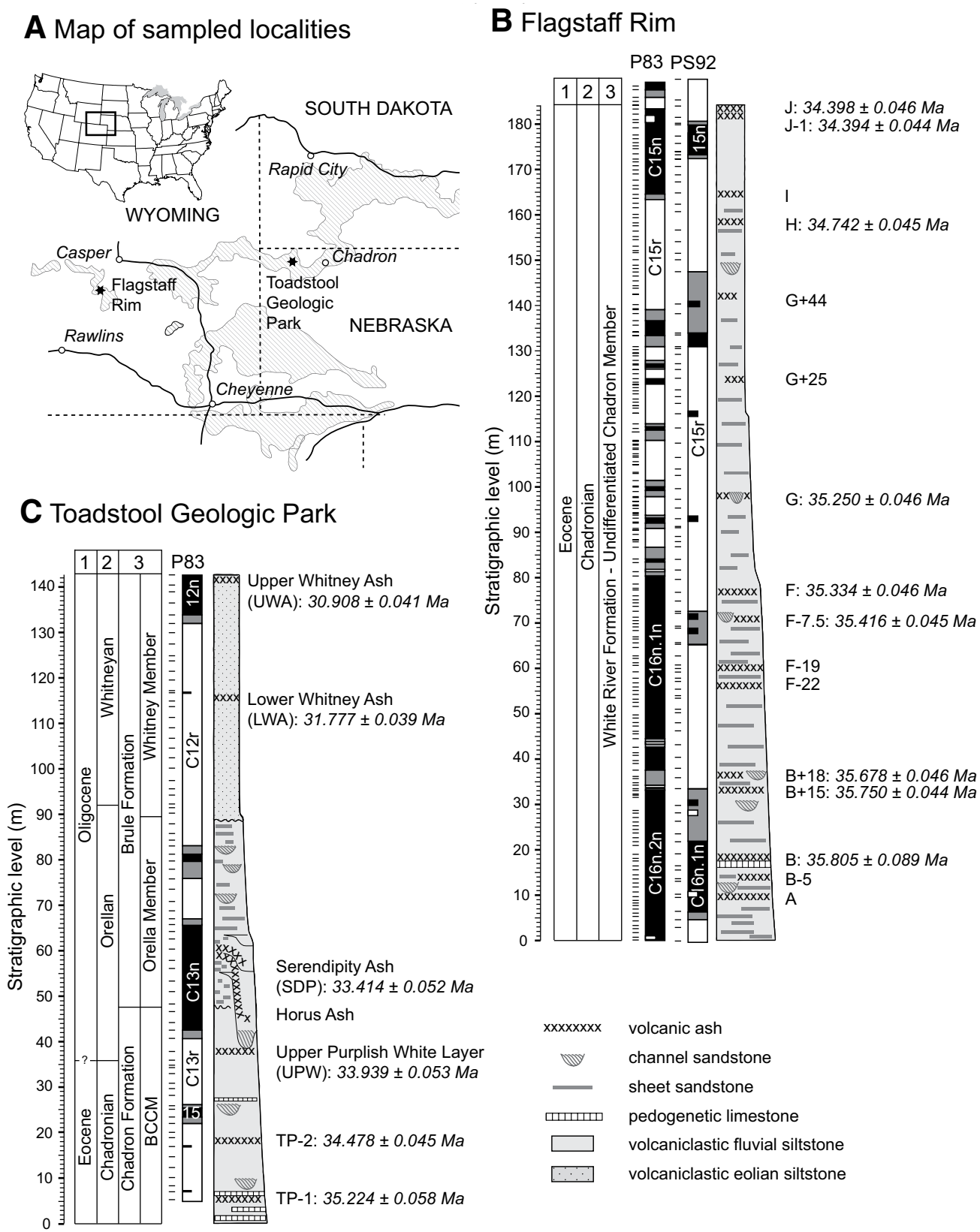

Figure 2. Lithostratigraphy, magnetostratigraphy and U-Pb geochronology of Flagstaff Rim and Toadstool Geologic Park. 1—age; 2—North American Land Mammal Age; 3—lithostratigraphy; P83—magnetic polarity record of Prothero et al. 1983; PS92—magnetic polarity record of Prothero and Swisher (1992) and Prothero (1985). Horizontal lines to the left of each magnetic polarity column indicate the approximate distribution of the analyzed paleomagnetic samples. Reprinted from Sahy et al. (2015), with permission from Elsevier, and modified to include the zircon $^{206}Pb/^{238}U$ dates of Sahy et al. (2015) listed with their total uncertainties (including isotopic tracer calibration and ^{238}U decay constant uncertainties) at the 2σ level.

Brule Formation is subdivided into the Orella, Whitney, and Brown Siltstone Members. The Orella Member consists of thinly interbedded brown and brownish-orange volcaniclastic overbank claystones and siltstones and bluish-green overbank sheet sandstone, while the Whitney Member mostly comprises pale-brown massive, nodular, eolian siltstones (LaGarry, 1998). The TGP sedimentary succession spans the Chadronian, Orellan, and Whitneyan NALMAs (late Eocene–early Oligocene; Prothero and Whittlesey, 1998), although boundaries between similarly named lithostratigraphic and biostratigraphic units do not necessarily coincide. A multi-storey Orellan (earliest Oligocene) channel complex incised ~20 m into the underlying Chadronian (late Eocene) deposits in the central part of TGP; however, the Chadronian–Orellan boundary interval is preserved outside the channel complex. Magnetostratigraphically, the TGP section spans three normal polarity zones correlated to C15n–C12n (Prothero and Swisher, 1992). This correlation is consistent with zircon $^{206}Pb/^{238}U$ dates from five tuffs intercalated in the TGP record (Sahy et al., 2015).

3. MATERIALS AND METHODS

Seven hundred and seventeen (717) oriented samples were collected at an average stratigraphic resolution of 0.5 m at FR and TGP, using a hand-held, generator-powered drill with a diamond-coated, water-cooled drill bit. One sample was collected per stratigraphic level. Samples were collected along sections spanning 5–50 m in stratigraphic thickness, correlated based on volcanic tuffs or prominent sandstone beds whose lateral continuity was verified visually. The location of the sections and the correlations between them are listed in Supplementary Tables S1 and S2[1], and visualized in the "Flagstaff_Rim.kmz" and "Toadstool_Geologic_Park.kmz" supplementary files. The latter include plots of sampled sections (blue) and outline the volcanic tuffs (red) and sandstone/limestone beds (green) used for correlation—labels for these features can be visualized by left-clicking on the respective plot element. Fresh rock was exposed by digging a 50-cm-wide and 50-cm-deep trench along each section, except for those spanning the Whitney Member of the Brule formation, where weathered material is removed by periodic flash floods along Big Cottonwood Creek. Sample positions were recorded using a Jacob staff and Abney level. Sample orientations were recorded using an orientation stage consisting of a clinometer, and a magnetic compass, and were corrected for present-day declination (–10° at FR, and –8° at TGP). Our FR composite section spans 183 m, starting 18.4 m below the B tuff, and ending at the J tuff of Emry (1973). Our TGP composite section spans 142 m, starting 38.3 m below the Upper Purplish White Layer and ending at the Upper Whitney Ash. Crucially, the stratigraphic positions of volcanic tuffs recorded in these composite sections form the basis for the $^{206}Pb/^{238}U$ calibrated age-depth models of the FR and TGP records (Sahy et al., 2015), and consequently the paleomagnetic and geochronologic data sets from the two localities are fully integrated.

Magnetic analysis was carried out at the Fort Hoofddijk Paleomagnetic Laboratory, Utrecht University. A first round of paleomagnetic analysis focused on 45 samples from FR and 35 samples from TGP, providing roughly evenly spaced coverage of both records at a stratigraphic resolution of ~4 m. This initial data set was then expanded by analyzing all available samples from stratigraphic intervals where preliminary data indicated the presence of magnetic reversals, and all available samples from intervals whose polarity could not be established based on the initial data set. The final data set included 185 samples from FR, equivalent to a mean temporal resolution of 8 k.y., and 157 samples from TGP, equivalent to a mean temporal resolution of 27 k.y. (Sahy et al., 2015). Samples were analyzed via stepwise demagnetization, with natural remanent magnetization (NRM) measured following each demagnetization step using a horizontal 2G Enterprise DC SQUID cryogenic magnetometer (noise level 3×10^{-12} Am^2). All samples were subjected to thermal demagnetization in a magnetically shielded oven at 100, 150, 200, and 240 °C in order to remove overprints carried by low blocking temperature minerals such as goethite alluded to by previous magnetostratigraphic studies of these records (Prothero et al., 1985; Prothero and Swisher, 1992). Approximately 60% of the samples were subjected to further thermal demagnetization using 30–40 °C temperature increments up to 660 °C. The remaining 40% of the samples were demagnetized using alternating field techniques in a 2G degausser, using 5 mT increments up to 40 mT, and then 10 mT increments up to a maximum intensity of 100 mT. Alternating field demagnetization was mainly used for stratigraphic intervals where thermal demagnetization above 270° resulted in unstable magnetic directions.

[1]GSA Data Repository item 2019238, which provides details of sampled localities, age modelling, uncertainty propagation, and summarises paleomagnetic results discussed in the text, is available at http://www.geosociety.org/datarepository/2019 or by request to editing@geosociety.org.

4. RESULTS

Demagnetization data were plotted on Zijderveld diagrams (Kirschvink, 1980; Zijderveld, 1967). The directions of different magnetic components were determined using best-fit lines with principal component analysis (Kirschvink, 1980) based on at least three consecutive demagnetization steps. Results are listed in Supplementary Tables S3 (FR) and S4 (TGP) (see footnote 1). Mean normal and reverse polarity directions were calculated using Fisher statistics (Fisher, 1953). Because WRG strata are broadly horizontal, no tectonic correction was applied.

4.1. Demagnetization Behavior

Initial NRM intensities ranged between 0.02 and 4 mA/m, increasing up-section at both localities. Eolian deposits above the I tuff at FR (Evanoff et al., 1992) and starting ~50 m above the Upper Purplish White Layer at TGP showed higher NRM values than the underlying fluvial deposits. All samples underwent thermal demagnetization up to a temperature of 240 °C. About 77% of the samples remained stable through this initial thermal demagnetization and retained ~20–30% of their original NRM at 240 °C.

Samples that were subjected to further thermal demagnetization above 240 °C generally yielded data that could be interpreted up to temperatures of 400–520 °C. Data from alternating field demagnetized samples could be interpreted up to field intensities of 70–90 mT. Samples that remained stable throughout the demagnetization process typically retained less than 10% of their original NRM signal when demagnetized at 660 °C or 100 mT, respectively. A low temperature component (LTC) with normal polarity is distinguishable in 96% of the samples, between 100 and 240 °C (Fig. 3). Mean declination (D) and inclination (I) of this component cluster close to the parameters of the present day magnetic field, which at the time of sampling was characterized by D = 10, I = 69 at FR, and D = 8, I = 69 at TGP (Fig. 4). Samples that remained stable above 240 °C exhibit a high temperature component (HTC) which steadily decays toward, but does not reach zero, and shows dual polarity. LTC (non-anchored fit) and HTC (anchored fit) were calculated using in-house software available from the Fort Hoofddijk Laboratory. Isolating the LTC and HTC in samples for which the latter shows normal polarity is difficult because the directions of the two components are nearly parallel. In samples for which the HTC shows reversed polarity, thermal demagnetization at 150–240 °C was sufficient to remove the LTC. For this reason,

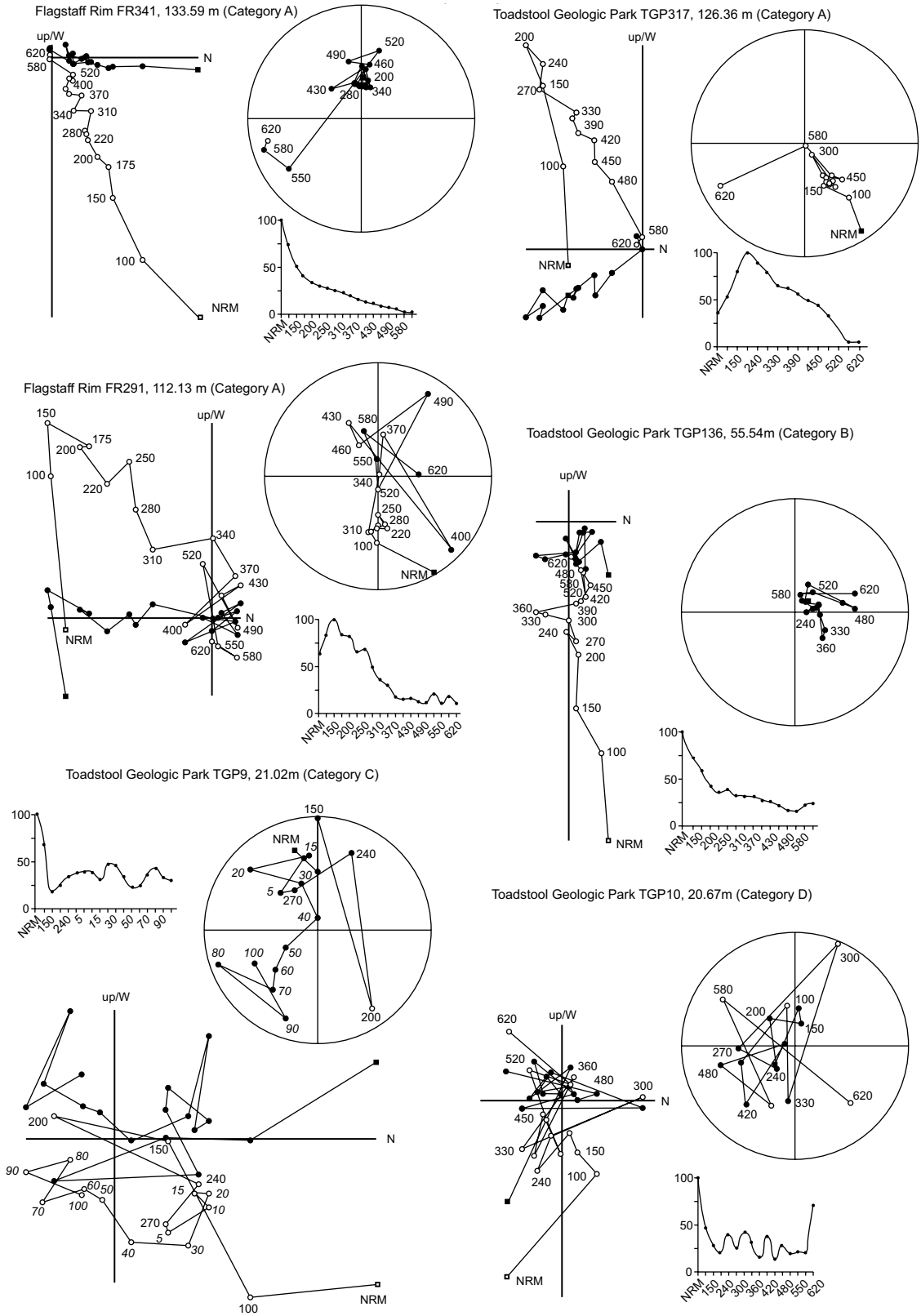

Figure 3. Representative Zijderveld diagrams for samples demagnetized using thermal (TGP317, TGP10, FR341, FR291, and FR1) and combined thermal and alternating field demagnetization techniques (TGP217). The stratigraphic position of each sample is indicated next to the diagrams. Closed (open) symbols denote the horizontal (vertical) component of the magnetic field, and squares indicate the initial natural remanent magnetization (NRM). Plain numbers indicate demagnetization temperature steps in °C. Numbers in italics indicate alternating field intensities in mT. A diagram showing the relative % decrease in magnetic moment with each demagnetization step is included for each sample. In terms of paleomagnetic interpretation, all samples fall in category A (see text for details) except FR1 and TGP10 (category D).

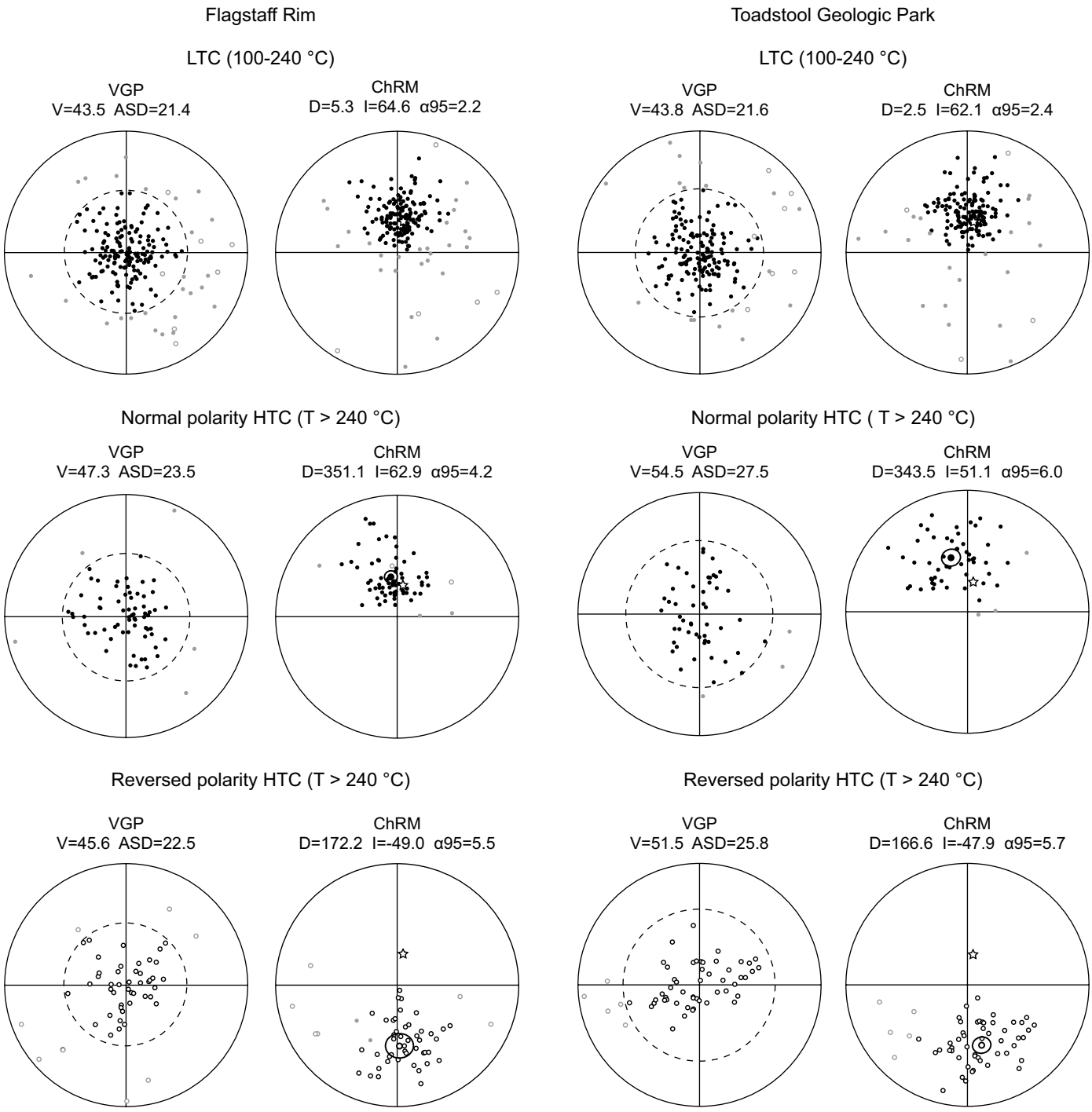

Figure 4. Equal area diagrams showing normal polarity low temperature component (LTC) and normal and reversed polarity high temperature components for the Flagstaff Rim and Toadstool Geologic Park records. Both the ChRM (characteristic remanent magnetization) and the calculated virtual geomagnetic pole (VGP) positions are shown. VGP plots are centered on the mean VGP for each sample group. D—mean declination; I—mean inclination; α95—95% confidence interval of the mean; V—angular cut-off distance from the mean VGP determined using the variable cut-off algorithm of Vandamme (1994) shown as dashed circle for each VGP plot; ASD—angular standard deviation of the mean VGP. Grey (category B)/black (category A) symbols represent data excluded from/included in the calculation of mean directions and VGP position based in the respective cut-off angles. Star indicates magnetic inclination and declination at the time of sampling.

all data obtained from thermal demagnetization steps below 240 °C in samples that showed a normal polarity HTC were attributed to present day overprint, while the HTC was defined based on data obtained above 240 °C. As the HTC shows dual, normal, and reversed polarity and appears to be carried by an iron oxide, such as magnetite, whose signal is likely to be of primary nature, it was interpreted as a primary characteristic remanent magnetization (ChRM) signal. Virtual geomagnetic pole (VGP) latitude data calculate base on the HTC of samples from FR and TGP showed high scatter, and were filtered using the variable cut-off algorithm of Vandamme (1994).

Samples were subdivided into four categories, A, B, C, and D (Supplementary Tables S3 and S4). Category D samples (~23% of the data set) were demagnetized to below a threshold of 0.02–0.05 mA/m during initial thermal demagnetization up to 240 °C, which usually resulted in unstable behavior with oscillating NRM intensities and directions. While most of these samples gave sufficient data to identify an LTC, no HTC could be calculated. Category C samples (9% of the data set) had an HTC with an associated mean angular deviation (MAD) in excess of 20°, and were excluded from interpretation. Category B samples (5% of the data set) were identified as outliers based on VGP data filtered through the Vandamme (1994) variable cut-off algorithm, and were also excluded. The remaining samples fell into category A (~63% of the data set) and were used to identify normal and reversed polarity intervals in the FR and TGP records.

4.2. Magnetic Polarity Record of the FR and TGP Sections

The magnetic polarity pattern of the FR and TGP sections was interpreted in terms of VGP latitudes. Changes in polarity were defined based pairs of at least two consecutive samples of identical polarity, and magnetic reversals were inferred to lie halfway between consecutive samples of opposite polarity. This approach identified seven polarity zones at FR and six at TGP, each of which was defined based on between 4 and 35 consecutive samples of the same polarity. Both the FR and TGP records include one or more 5–15-m-thick intervals of indeterminate polarity, which most likely result from an incomplete removal of weathered material during sampling. In spite of this, the stratigraphic positions of most magnetic reversal were constrained to better than ±2 m (Figs. 5 and 6).

4.2.1. Flagstaff Rim

Our interpretation of the FR magnetic polarity record, which comprises four normal and three

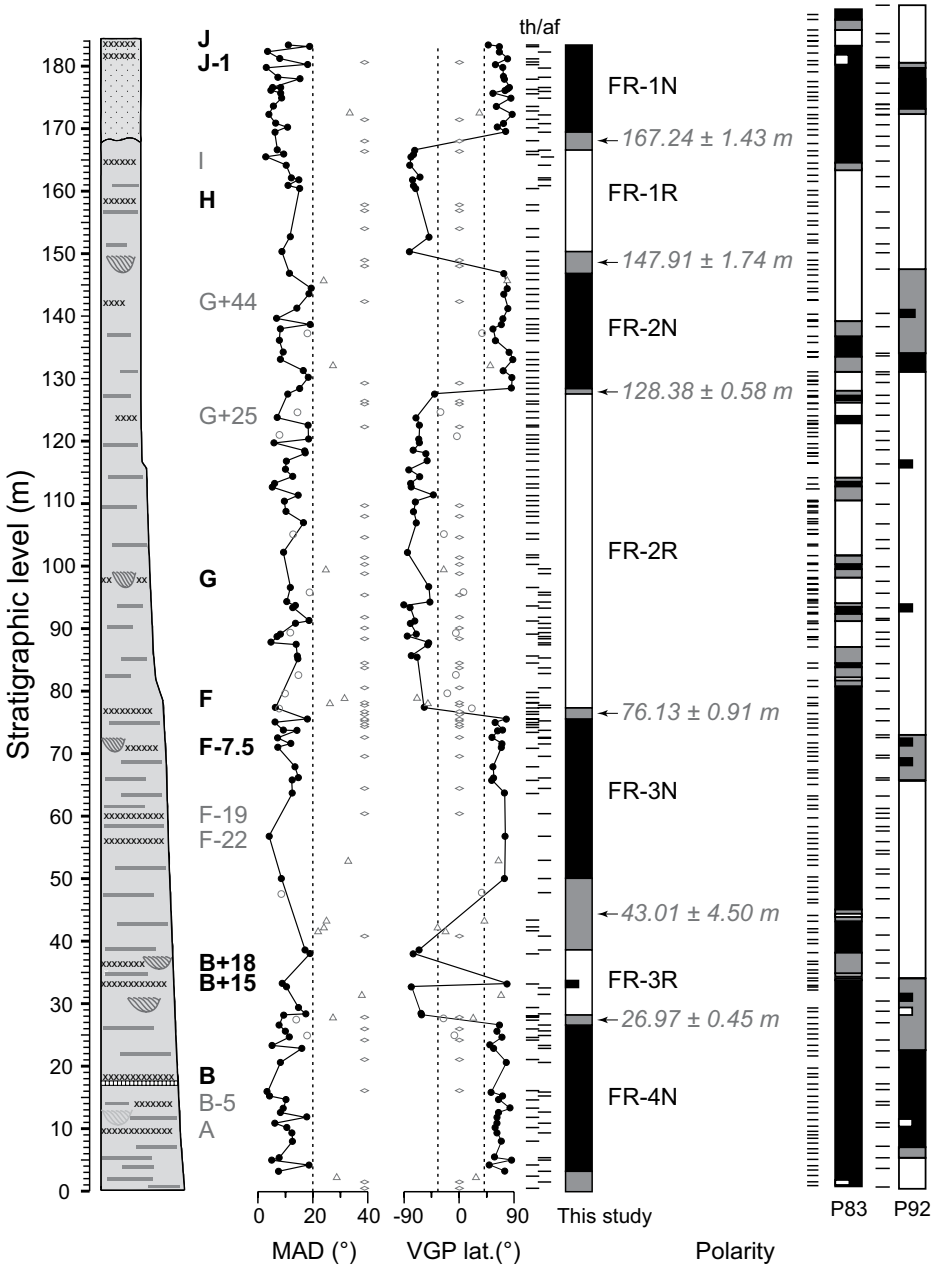

Figure 5. Magnetostratigraphy of the Flagstaff Rim section. Mean angular deviation (MAD) and virtual geomagnetic pole latitude (VGP lat.) are plotted for each sample. Diamonds—category D samples showing unstable magnetic directions above 240 °C; triangles—category C samples, with MAD > 20°; open circles—category B samples excluded through filtering of VGP data using the variable cut-off algorithm of Vandamme (1994), closed circles—category A samples underpinning the interpretation of the magnetic polarity pattern. Black, white, and gray intervals in the polarity column represent normal, reverse and indeterminate polarity respectively. P83—magnetostratigraphic interpretation of Prothero et al. (1983); P92—magnetostratigraphic interpretation of Prothero (1985) and Prothero and Swisher (1992). Horizontal lines next to each polarity column indicate the approximate distribution of paleomagnetic samples. For this study, lines offset to the left (right) indicate the use of thermal (alternating field) techniques to derive the ChRM (characteristic remanent magnetization) of each sample.

reversed intervals (Fig. 5), differs significantly from earlier studies. Prothero et al. (1982, 1983) determined that the lower half of the section, below the F tuff, recorded mostly normal polarity, based on analyzing a set of samples with a mean stratigraphic resolution of 0.8 m using alternating field demagnetization. Prothero (1985) analyzed a second group of samples, with sets of three replicates collected at a mean stratigraphic resolution of 1.7 m, using thermal demagnetization. The resulting record was dominated by reversed polarity, with two short normal polarity intervals identified in the vicinity of the B tuff and between the I and J tuffs. The discrepancies between these two early interpretations were attributed to the incomplete removal of present-day field overprints (Prothero 1985; Prothero and Swisher, 1992). Such overprints were thought to be carried by low blocking temperature but high coercivity minerals (e.g., goethite), resulting in spurious normal polarity zones in the Prothero et al. (1982, 1983) studies, which used alternating field demagnetization. Because all samples from the present study were thermally demagnetized up to at least 240 °C, such overprints are unlikely to have a significant impact on our interpretation. Furthermore, our FR polarity record consists of interspaced samples for which the HTC was analyzed using thermal and alternating field demagnetization respectively (except between the H and G tuffs where only thermal demagnetization was used) and no systematic differences were detected between results obtained using the two methods. However, the lack of normal polarity zones between the B+15 and H tuffs in the data of Prothero et al. (1985) remains puzzling. Assuming the zircon $^{206}Pb/^{238}U$ geochronology of Sahy et al. (2015) is correct, such zones would be expected to occur based on the late Eocene polarity record of the UMB, ATPS06, and PEAT (see Sections 5.1 and 5.2). It is unlikely that the data set of Prothero et al. (1985) includes samples with reverse polarity overprints, given that no evidence of such artifacts has been found in our own samples. It seems equally unlikely that processes such as lightning strikes would have consistently reset the magnetic signal over several tens of meters of stratigraphy. However, given the topography of the FR area, assembling a continuous collection of paleomagnetic samples between the B and J tuffs must rely on individual measured sections correlated based on volcanic tuffs or other prominent beds (see Section 3, and Tables S1 and S2). As a result, it is possible that errors in such correlations have resulted in normal polarity zones being missed in the data set of Prothero et al. (1985).

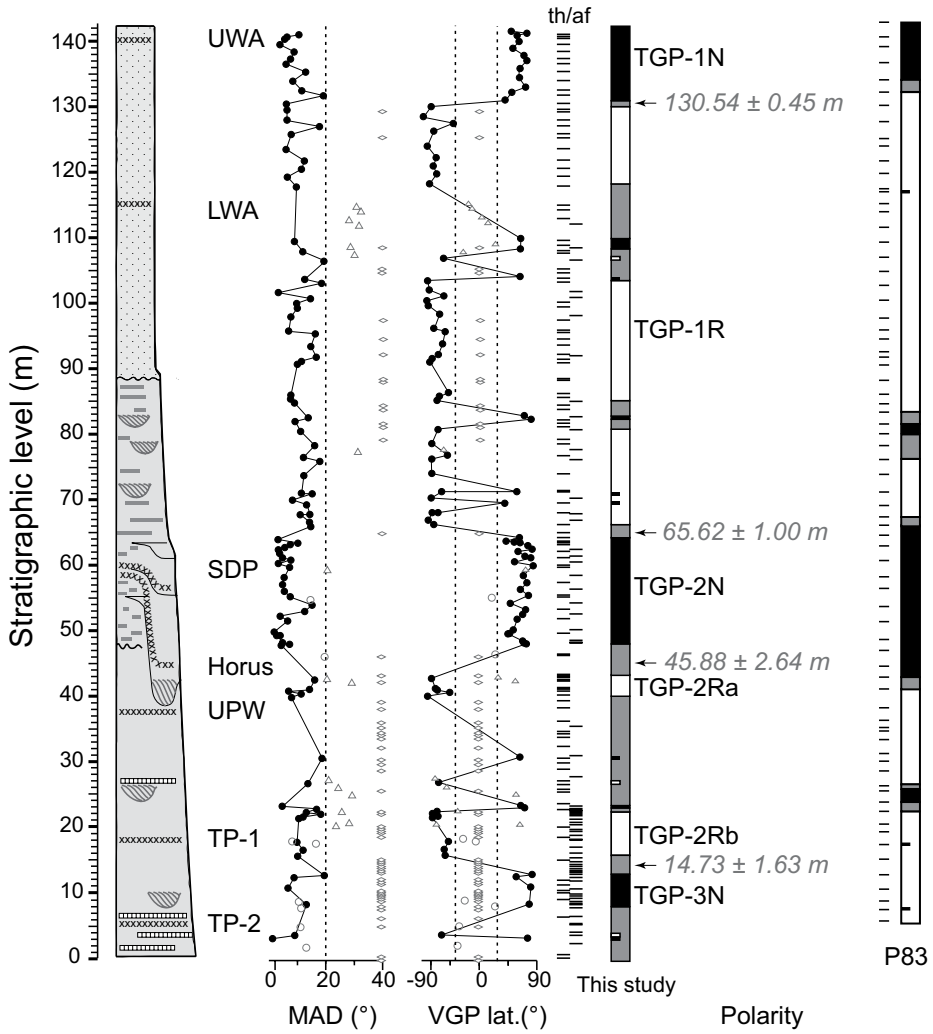

Figure 6. Magnetostratigraphy of the Toadstool Geologic Park section. All symbols are the same as in Figure 5. Magnetostratigraphic interpretation of Prothero et al. (1983) (P83) is shown for comparison. UWA—Upper Whitney Ash; LWA—Lower Whitney Ash; SDP—Serendipity ash; UPW—Upper Purplish White Layer; TGP—Toadstool Geologic Park; MAD—mean angular deviation; VGP—virtual geomagnetic pole latitude.

The mean direction of normal polarity samples was D = 351.1, I = 62.9, and that of reversed polarity samples was D = 172.2, I = –49.0. For comparison, the expected normal polarity directions for the FR site varied from D = 344.3, I = 62.4 at 36 Ma to D = 345.3, I = 63.2 at 34 Ma (Besse and Courtillot, 2002; Tauxe, 2010).The Flagstaff Rim samples failed the reversal test of Tauxe (2010) due to a difference of 11° between mean normal and reversed polarity inclinations. Such non-antipodal directions in Cenozoic sediments may be attributed to the presence of partially unremoved present day overprints, or persistent non-dipole contributions to the magnetic field during reversed polarity intervals (e.g., Parés and Van der Voo, 2013). In spite of the non-antipodal nature of the mean normal and reversed directions in the FR record, we nonetheless interpret the ChRM as a primary signal due to: (*i*) its dual polarity, (*ii*) the fact that thermomagnetic runs (Mullender et al., 1993) suggest that magnetization is carried by magnetite, whose signal is likely to be of primary nature (Fig. S1; see footnote 1), and (*iii*) because, as discussed below in Sections 5.1 and 5.2, except for zone FR1N, the placement, and implicitly the age of the normal polarity zones conforms to what we would expect based on late Eocene magnetic polarity records from the UMB, ATPS06 and PEAT data sets.

4.2.2. Toadstool Geologic Park

In the lower 40 m of the TGP record, samples yielding reliable magnetic directions form

distinct clusters around 3, 8, 12, 18, and 21–28 m (n = 23, out of 71 analyzed samples; Fig. 6). The quality of the data improves significantly around 47 m above the base of the section, or ~8 m above the Upper Purplish White Layer , which broadly coincides with the lithological boundary between the Chadron and Brule formations. Our interpretation of the TGP magnetic polarity record comprises three normal and two reversed polarity zones, and is generally in agreement with earlier work by Prothero et al. (1983), except for a short normal polarity zone in the lower part of the section (TGP-3N in Fig. 6) which has not been previously reported. Normal and reversed polarity directions passed the reversal test of Tauxe (2010); however, mean inclinations are ~10° lower than expected from plate tectonic models (Torsvik et al., 2008) indicating some degree of post-depositional compaction. The mean direction of normal polarity samples was D = 343.5, I = 51.1, and that of reversed polarity samples was D = 166.6, I = –47.9. For comparison, the expected normal polarity directions for the FR site varied from D = 344.2, I = 62.4 at 36 Ma to D = 345.9, I = 63.9 at 31 Ma (Besse and Courtillot, 2002; Tauxe, 2010).

5. DISCUSSION

5.1. Correlation of the WRG Record to the GPTS

Historically, the published magnetic polarity pattern of the FR and TGP sections has been correlated to chrons C12n–C16n.1n of the GPTS (Prothero and Swisher, 1992) based on the $^{40}Ar/^{39}Ar$ dates of Swisher and Prothero (1990). More recently, $^{206}Pb/^{238}U$ dating of zircons from 15 tuffs intercalated in the FR and TGP records (Sahy et al., 2015) has demonstrated that the $^{40}Ar/^{39}Ar$ dates of Swisher and Prothero (1990) were anomalously old by up to 0.6 m.y., likely due to the inadvertent analysis of older detrital biotite and anorthoclase grains. Consequently, our attempts to refine the correlation of magnetic polarity patterns identified in this study to the GPTS are based on the $^{206}Pb/^{238}U$ calibrated age-depth models of Sahy et al. (2015), which rely on the Bayesian approach implemented in the OxCal software package of Bronk-Ramsey (2008), and are described in Section S1 of the Supplementary Materials (see footnote 1). Magnetic reversal ages extracted from these age depth models (Table 1) and compared to the independently dated UMB, APTS06 and PEAT records are used to correlate the polarity pattern identified at FR and TGP to the GPTS, and to develop a composite polarity record for the late Eocene–early Oligocene portion of the WRG (Fig. 7). Data from the geological time scale were not included in these comparisons, as the radio-isotopic age model presented therein relied on anomalously old $^{39}Ar/^{40}Ar$ dates from the UMB (Sahy et al., 2017) and the late Eocene portion of their astronomically tuned Paleogene GPTS relied on interpolation rather than direct dating of magnetic reversals. All volcanic tuff age quoted in the following discussion were obtained using the $^{206}Pb/^{238}U$ isotope system, and are accompanied by their total propagated uncertainty (including ^{238}U decay constant and isotopic tracer composition uncertainties). All interpolated magnetic reversal ages are quoted with their full uncertainty (Equation S3; see footnote 1), the bulk of which stems from the uncertainty of the U-Pb-calibrated age depth model, while stratigraphic uncertainties account for less than one third of the uncertainty budget.

At TGP, the base of polarity zone TGP-1N is bracketed by the upper and Lower Whitney Ashes (30.91 ± 0.04 Ma and 31.78 ± 0.04 Ma, respectively), with an interpolated age of 31.28 ± 0.17 resulting in an unambiguous correlation to the base of C12n. The top of polarity zone TGP-2N is bracketed by the Lower Whitney Ash and the Serendipity tuff (33.41 ± 0.05 Ma) with an interpolated age of 33.29 ± 0.15 Ma. The base of zone TGP-2N is bracketed by the Serendipity tuff and the Upper Purplish White Layer (33.94 ± 0.05 Ma) and has an interpolated age of 33.69 ± 0.21 Ma. Based on the above, zone TGP-2N correlates to chron C13n in the UMB, ATPS06 and PEAT records. Zone TGP-3N is bracketed by the TP-2 tuff (34.48 ± 0.05 Ma) and the TP-1 tuff (35.22 ± 0.06 Ma) with interpolated age of 34.83 ± 0.11 for its top, while its base could not be identified.

At Flagstaff Rim, polarity zone FR-1N is bracketed by the J (34.40 ± 0.05 Ma) J-1 (34.39 ± 0.04 Ma) and H (34.74 ± 0.05 Ma) tuffs. The base of zone FR-1N has an interpolated age of 34.64 ± 0.11 Ma, and its top could not be identified. This polarity zone has been identified in both previous interpretations of the FR magnetic polarity record (Prothero et al., 1982, 1983; Prothero 1985) and has been correlated to C15n based on the $^{40}Ar/^{39}Ar$ data of Swisher and Prothero (1990). However, when calibrated using the U-Pb data of Sahy et al. (2015), this zone appears to fall between the positions of C15n and C13n in the UMB, ATPS06, and PEAT records. At TGP, the corresponding interval lies between meter levels 15.50 and 21.25 and is of reversed polarity. Consequently, zone FR-1N may correspond to a normal polarity sub-chron within C13r that is older than the C13r.1n identified in the ATPS06 (Pälike et al., 2006), or may reflect incomplete removal of a present-day normal polarity overprint. The latter is difficult to assess, given that normal polarity ChRM for this data set has a similar orientation to the present day-field. Zone FR-2N, not reported in previous interpretations of the FR magnetic polarity pattern, is bracketed by the H and G tuffs (34.74 ± 0.05 Ma and 35.25 ± 0.05 Ma, respectively), with an interpolated age of 34.83 ± 0.11 for its top and 34.99 ± 0.12 for its base. These ages are closely aligned with the position of zone TGP-3N in the TGP section and suggest a correlation

TABLE 1. AGE OF MAGNETIC REVERSALS BETWEEN C12N AND C16N.2N BASED ON THE WRG, UMB, ATPS06 AND PEAT RECORDS

Reversal	WRG	UMB	ATPS06	PEAT
C12n_base	31.28 ± 0.15/0.15/0.17	31.23 ± 0.07/0.08/0.12	31.03 ± 0.05/0.06/0.06	30.98 ± 0.05/0.06/0.08
C13n_top	33.29 ± 0.12/0.13/0.15	33.10 ± 0.06/0.06/0.07	33.16 ± 0.05/0.06/0.06	33.21 ± 0.05/0.06/0.06
C13n_base	33.69 ± 0.13/0.14/0.21	33.74 ± 0.12/0.13/0.17	33.71 ± 0.05/0.06/0.06	33.73 ± 0.05/0.06/0.07
C15n_top	34.83 ± 0.09/0.10/0.11	34.91 ± 0.06/0.07/0.08	35.13 ± 0.05/0.06/0.07	35.10 ± 0.05/0.06/0.09
C15n_base	34.99 ± 0.11/0.12/0.12	35.11 ± 0.06/0.07/0.08	35.25 ± 0.05/0.06/0.11	35.34 ± 0.05/0.06/0.08
C16n.1n_top	35.37 ± 0.04/0.06/0.07	35.43 ± 0.03/0.05/0.05	35.33 ± 0.05/0.06/0.07	35.58 ± 0.05/0.06/0.08
C16n.1n_base	35.63 ± 0.06/0.07/0.11	35.50 ± 0.03/0.05/0.11	35.55 ± 0.05/0.06/0.07	35.72 ± 0.05/0.06/0.08
C16n.2n_top	35.78 ± 0.05/0.07/0.09	35.68 ± 0.06/0.07/0.15	35.64 ± 0.05/0.06/0.07	35.77 ± 0.05/0.06/0.08

Notes: Uncertainties are quoted as ± X/Y/Z where X is the U-Pb based age model uncertainty (White River group [WRG], Umbria-Marche basin [UMB]) or tuning uncertainty (ATPS06, Pacific Equatorial Age Transect [PEAT]), Y is the age uncertainty including systematic components related to U-Pb dating and astronomical tuning (Equations S1 and S2; see text footnote 1), and Z includes the stratigraphic uncertainty of each reversal in the respective record (Equations S3 and S4; see text footnote 1). The stratigraphic uncertainty of the UMB record was estimated based on the work of Jovane et al., 2006, Hyland et al. (2009) and Coccioni et al. (2008). Stratigraphic uncertainties for the ATPS06 are based on the compilation of Westerhold et al. (2012) quantified assuming a mean sediment accumulation rate of 10 m/m.y.—where the same reversal is recorded in multiple cores, the lowest stratigraphic uncertainty was selected. Stratigraphic uncertainties on the PEAT age model are based on Westerhold et al. (2014).

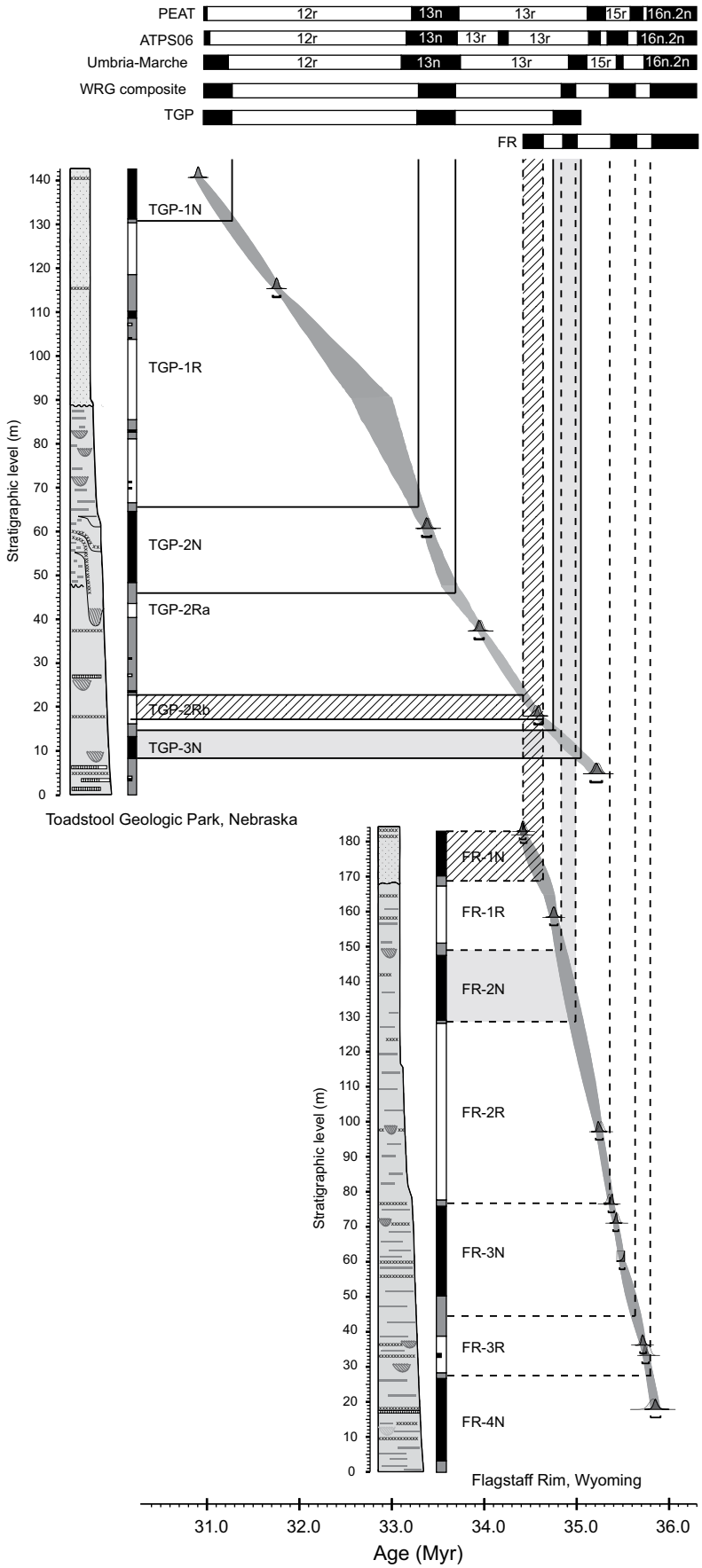

to C15n when compared with the UMB record, although they are slightly younger than would be expected based on the ATPS06 and PEAT data set (Fig. 7). Zone FR-3N is bracketed by the F (35.33 ± 0.05 Ma) and B+18 tuffs (35.68 ± 0.05 Ma) and includes the F-7.5 tuff (35.42 ± 0.05 Ma). The interpolated age for the top and base of zone FR-3N are 35.37 ± 0.07 and 35.63 ± 0.11 Ma respectively, suggesting a correlation with C16n.1n in the UMB, ATPS06 and PEAT records. The top of zone FR-4N is bracketed by the B+15 (35.75 ± 0.04 Ma) and B tuffs (35.81 ± 0.09 Ma), placing its interpolated age at 35.78 ± 0.09 Ma which indicates a correlation with chron C16n.2n.

Based on the above, the magnetic polarity pattern of the FR and TGP sections, which covers the interval between 30.9 and 35.8 Ma, correlates to chrons C12n–C16n.2n of the GPTS. The two records overlap between 35.2 and 34.4 Ma, which includes normal polarity zones correlated to C15n at both localities. Mean sediment accumulation rates for this overlapping interval are around 60–130 m/m.y. at FR and 18–30 m/m.y. at TGP (Sahy et al., 2015). This, combined with our sampling strategy, results in a considerably higher resolution record of C15n at FR, compared to TGP, where the base of C15n could not be identified. As a result, our composite magnetic polarity record of the WRG (Fig. 7) is based on data from TGP between 30.9 and 34.4 Ma and data from FR between 34.4 and 35.8 Ma.

5.2. Comparison with Astronomically Tuned Records of the Late Eocene–Early Oligocene

Magnetic reversals take place over a few thousand years (Clement, 2004) and consequently,

Figure 7. Correlating the magnetic polarity pattern of the Flagstaff Rim and Toadstool Geologic Park (TGP) section to the geomagnetic polarity time scale using the U-Pb calibrated Umbria-Marche basin (UMB) record as a reference. Grey bars show correlation between normal polarity zones FR-2N, TGP-3N, and C15n in the UMB record. Hatched bars show the reversed polarity intervals equivalent to zone FR-1N in the TGP, UMB, ATPS06, and PEAT (Pacific Equatorial Age Transect) records. The composite White River Group (WRG) magnetic polarity record is based on the location of C13n and C12n at TGP, and the location of C16n.2n, C16n.1n and C15n at Flagstaff Rim (FR).

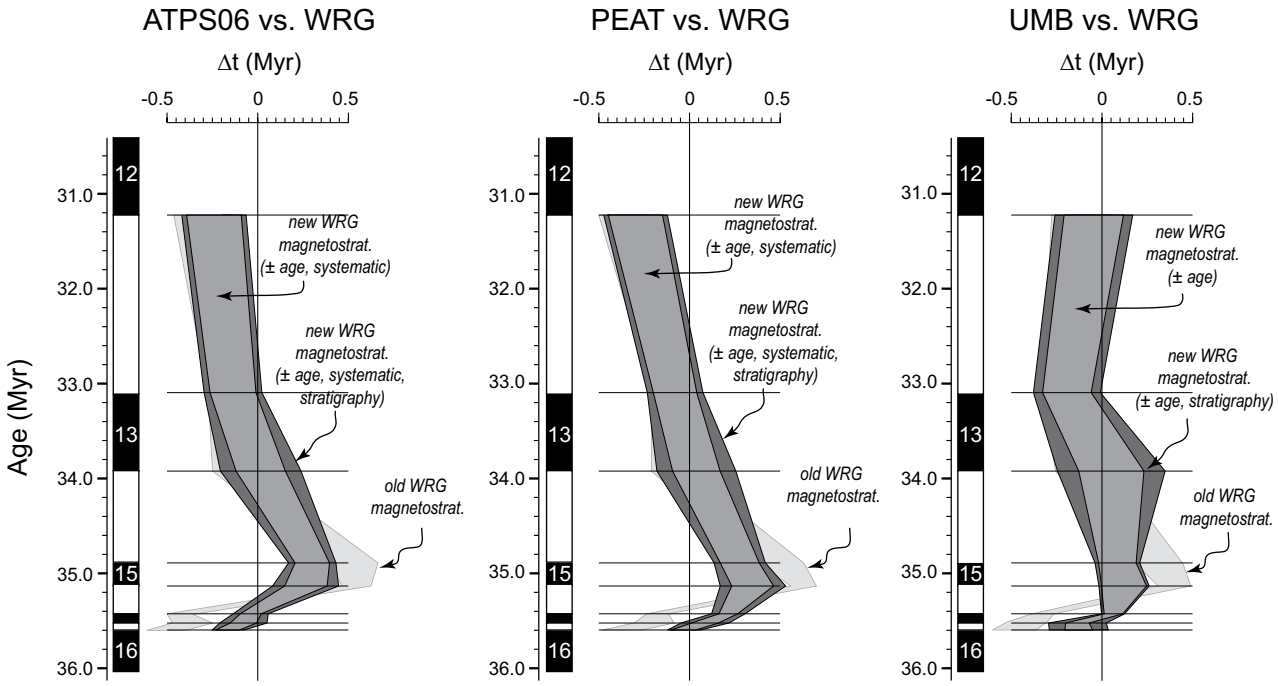

Figure 8. Comparison between the revised magnetostratigraphy of the White River Group (WRG) calibrated using the $^{206}Pb/^{238}U$ zircon dates of Sahy et al. (2015), the astronomically tuned ATPS06 and Pacific Equatorial Age Transect (PEAT) records, and the $^{206}Pb/^{238}U$ calibrated magnetostratigraphy of the Umbria-Marche basin (UMB). Age uncertainties were propagated based on Equations S5 and S6 (dark gray uncertainty envelope). To illustrate the impact of stratigraphic uncertainties, light gray uncertainty envelopes were plotted assuming stratigraphic uncertainties were zero. Stratigraphic uncertainties were quantified based on this study for the WRG record, the magnetostratigraphy of Jovane et al. (2006) and Hyland et al. (2009) for the UMB record, and the magnetostratigraphy of Sites 1218, 1219, and 1220 of ODP Leg 199 as summarized by Westerhold et al. (2012) for the ATPS06, and table 1 of Westerhold et al. (2014) for the PEAT. The age difference between the previously published magnetostratigraphy of the WRG (Prothero et al. 1983; Prothero and Swisher 1992) and the UMB, ATPS06, and PEAT records is plotted in the background for comparison.

they can be regarded as instantaneous within the resolution afforded by astronomical tuning and $^{206}Pb/^{238}U$ dating in the EOT interval. It then follows that the same reversal recorded at different localities and dated using different methods should appear as synchronous if the dating results and the age models built upon them are accurate, and all uncertainties are adequately quantified. Age control for the magnetic reversals recorded in the WRG and UMB successions is based on the $^{206}Pb/^{238}U$ dating of zircons from volcanic tuffs (Sahy et al., 2015, 2017). Systematic bias between age data from these two records can be ruled out as the dating is based on the same isotope system, and was carried out in the same laboratory, using the same isotopic tracer, measured on the same instrument, within the same three-year time frame, and interpreted by the same analyst using the same statistical approach. Nonetheless, some discrepancies in excess of our calculated 95% confidence intervals are evident between these two records when considering age model uncertainties alone (Fig. 8; Tables 1, 2). However, additional uncertainties arise from the resolution of the respective magnetostratigraphic records, which determines how precisely the stratigraphic position of a magnetic reversal can be identified. In the WRG record, these stratigraphic uncertainties vary between ±0.45 and 4.50 m, which translates to ±5–75 k.y. (Sahy et al., 2015). For the UMB record, the stratigraphic uncertainty varies between 8 and 82 k.y. (Sahy et al., 2017). The propagation of analytical, systematic and stratigraphic uncertainties relevant to each reversal is discussed in the Supplementary Material, Section S2 (see footnote 1). All uncertainty components are summarized in Table S5 (see footnote 1). Once stratigraphic uncertainties are considered, magnetic reversals

TABLE 2. AGE OFFSET BETWEEN THE WRG AND THE ATPS06, PEAT, AND UMB RECORDS

Reversal	ATPS06 vs. WRG	PEAT vs. WRG	UMB vs. WRG
C12n_base	–0.24 ± 0.15/0.18	–0.30 ± 0.16/0.19	–0.05 ± 0.16/0.22
C13n_top	–0.14 ± 0.13/0.16	–0.08 ± 0.14/0.16	–0.19 ± 0.13/0.18
C13n_base	0.02 ± 0.14/0.23	0.04 ± 0.15/0.23	0.05 ± 0.18/0.30
C15n_top	0.30 ± 0.10/0.14	0.28 ± 0.11/0.16	0.09 ± 0.10/0.12
C15n_base	0.27 ± 0.12/0.19	0.35 ± 0.13/0.15	0.12 ± 0.12/0.14
C16n.1n_top	–0.04 ± 0.07/0.10	0.21 ± 0.08/0.11	0.06 ± 0.05/0.06
C16n.1n_base	–0.08 ± 0.08/0.14	0.09 ± 0.09/0.15	–0.13 ± 0.07/0.16
C16n.2n_top	–0.17 ± 0.07/0.10	–0.03 ± 0.09/0.11	–0.13 ± 0.08/0.16

Notes: Positive/negative numbers indicate the age calculated based on the White River Group (WRG) record is younger/older than the record to which the comparison is made. Uncertainties are reported as ± A/B where A encompasses the relevant U-Pb age model, tuning uncertainties and systematic uncertainties, and B is the total uncertainty including a stratigraphic component (Equations S5 and S6; see footnote 1). PEAT—Pacific Equatorial Age Transect; UMB—Umbria-Marche basin.

from the WRG and the UMB appear to be synchronous except for the top of C13n, where the offset is 193 ± 184 k.y. This is an argument in favor of the accuracy of the U-Pb dates underpinning the WRG and UMB records. The interpretation of $^{206}Pb/^{238}U$ data from each volcanic tuff is based upon a weighted mean age of statistically equivalent analyses. These weighted means could include grains whose age was influenced by geological processes such as subtle Pb-loss (younger age) or prolonged crystallization (older age) at a level that is masked by the 2σ uncertainties of the respective analyses. However, agreement between magnetic reversal ages calculated from the WRG and UMB would suggest that neither U-Pb-calibrated age model contains significant errors. Conversely, if significant errors were present in the two age models, then this would require zircon data from tuffs sourced from unrelated volcanic provinces to be affected by the same amount of geological bias toward younger/older ages (within uncertainty), which seems unlikely.

In addition to stratigraphic uncertainties, systematic uncertainties related to the calibration of isotopic tracers used in U-Pb dating (~0.03%), the value of the ^{238}U decay constant (~0.11%) and the numerical insolation models that underpin astronomical tuning (~0.1%) must also be taken into account when comparing magnetic reversal ages obtained using U-Pb dating and astronomical tuning.

When comparing the WRG composite to ATPS06 and PEAT records, small discrepancies become evident for all reversal in the C12n–C16n.2n range, except for the boundaries of C13n, even after all sources of uncertainty are taken into account (Fig. 8). For some chron boundaries, the U-Pb calibrated age is older than that derived from astronomically tuned age models, while the reverse is true for other chrons. This is similar to data from the Miocene La Vedova and Monte dei Corvi sections in Italy that showed no systematic offset between independent astronomical tuning (Hüsing et al., 2009, 2010) and $^{206}Pb/^{238}U$ dating of volcanic tuffs (Wotzlaw et al., 2014). The base of C12n and both boundaries of C15n are examples where there is agreement between the astronomically tuned ATPS06 and PEAT models, and between the WRG and UMB records, but the offset between nominal ages derived using different dating methods is up to 300 k.y. Agreement with astronomically tuned age models is reached for two out of the three oldest reversals recorded in the WRG, with discrepancies at the top of C16n.2n relative to the ATPS06, and top of C16n.1n relative to the PEAT. The implication is that although the ATPS06 and PEAT astrochronologies appear to diverge below the base of C15n (Fig. 1), a comparison with our U-Pb calibrated chron boundaries cannot be used to pinpoint either model as more accurate. Furthermore, if the magnetic polarity patterns underpinning the ATPS06 and PEAT records are assumed to be free of errors, then discrepancies between the two age models must arise from the tuning process itself, in which case the age uncertainties quoted from these records are significantly underestimated. This, along with magnetic reversal ages calculated from the UMB and WRG records suggests that in spite of the application of dating methods whose theoretical precision approaches 0.1%, the age of most late Eocene–Oligocene magnetic reversals cannot, at present, be constrained to better than ± 100–150 k.y. (0.3–0.5%).

5.3. Late Eocene–Early Oligocene Seafloor Spreading Rates

The assumption of smoothly varying seafloor spreading rates has been fundamental to the development of the radio-isotopically calibrated GPTS (e.g., Cande and Kent, 1992, 1995; Berggren et al., 1985; Ogg and Smith, 2004; Vandenberghe et al., 2012). The same assumption has been widely used to test the validity of astronomically calibrated magnetic reversal ages (e.g., Wilson, 1993; Krijgsman et al., 1999; Beddow et al., 2018). A similar test can be used to evaluate the radio-isotopic or astronomical dating of the WRG, UMB, ATPS06 and PEAT records by calculating apparent spreading rates based on the South Atlantic anomaly profile of Cande and Kent (1992) (Fig. 9). The caveat is that for chrons shorter than a few 100 k.y., even small errors in the age of chron boundaries can lead to large jumps in apparent seafloor spreading rates. As an example, the ATPS06 exhibits an increase in apparent spreading rates during chron C15, the duration of which is estimated around 200 k.y., compared to ~500 k.y. in the WRG, UMB and PEAT records. There is also a large offset in the duration of chron C13 between the WRG (~1.54 m.y.) and the UMB (1.81 m.y.), ATPS06 (1.97 m.y.), and PEAT (1.89 m.y.) (Fig. 9). At a first glance, this would suggest the presence of a spurious 405 k.y. cycle in the ATPS06 and PEAT records. However, this is unlikely, as such an error in the tuning is not consistent with our comparisons between U-Pb calibrated and astronomically tuned ages for the boundaries of chron C16n.1n and C16n.1r (Fig. 8). Instead, the source of this offset is more likely to be either errors in the location of chron boundaries, or changes in sedimentation rate that were not adequately accounted for in either the U-Pb calibrated or astronomically tuned records.

For the WRG, spreading rates calculated for chrons C12r, C13, C15, and part of C16 (i.e., C16n.1n and C16n.1r) are statistically equivalent. For the ATPS06 and PEAT records, scatter in apparent seafloor spreading rates is at least in part due to the comparatively higher precision of the astronomically tuned age models, and the higher stratigraphic resolution of the underpinning magnetostratigraphic records, which leads to more precise calculated spreading rates (details on the propagation of spreading rate uncertainties are discussed in the Supplementary Material, Section S2). Although the interval covered here is admittedly relatively short, this does nonetheless raise the question whether the uncertainties of the astronomically tuned age models are underestimated.

6. CONCLUSIONS

The precision of state-of-the-art dating methods such as $^{206}Pb/^{238}U$ zircon geochronology and astronomical tuning approaches 0.1% (30–40 k.y.) in the Paleogene. However, when these methods are applied to potentially complex stratigraphic records and proxy data, additional sources of error and uncertainty come into play. We explored these using the calibration of the late Eocene–early Oligocene portion of the GPTS as a case study. First, we revised the magnetostratigraphy of the FR and TGP sections of the WRG, which are among the most thoroughly dated terrestrial records of the EOT, with published interpolated age models based on the $^{206}Pb/^{238}U$ isotope system. This led to adjustments in the positions of boundaries between chrons C13r and C16n.2n, and resulted in interpolated magnetic reversal ages that are in agreement with those derived from the $^{206}Pb/^{238}U$-dated Rupelian and Chattian GSSP sections in the UMB. Some discrepancies persist between $^{206}Pb/^{238}U$ dated records of the EOT, and the astronomically tuned ATPS06 and PEAT records, in spite of our attempts to account for systematic uncertainties inherent to both dating methods and stratigraphic uncertainties related to the position of magnetic reversals at each locality. These discrepancies may arise from errors in dating and/or age model development, or the identification of magnetic reversals in any of the four records considered in this study. However, agreement between the U-Pb-dated WRG and UMB records and the presence of discrepancies between the ATPS06 and PEAT data sets would suggest that the uncertainties associated with the astronomically tuned records of the EOT have been underestimated. The implication is that, at present, even applying state-of-the-art dating techniques, it does not appear to be possible to quantify the age of magnetic reversals in

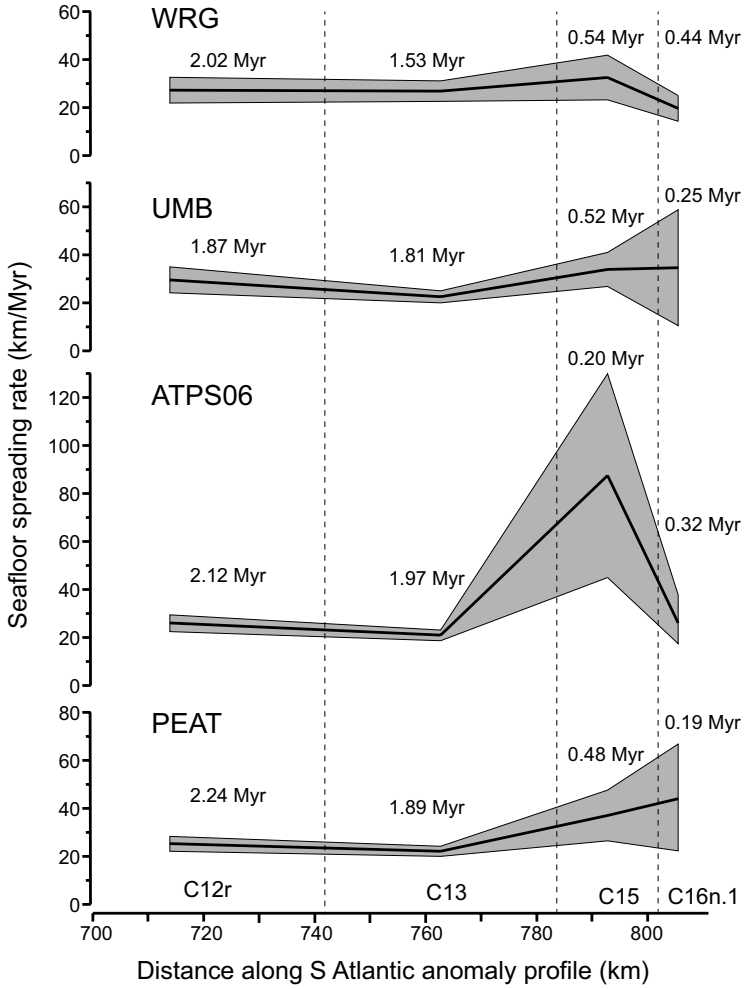

Figure 9. Mean seafloor spreading rates calculated by plotting magnetic reversal ages from the White River Group (WRG), Umbria-Marche basin (UMB), ATPS06, and Pacific Equatorial Age Transect (PEAT) records against the synthetic marine magnetic anomaly profile of Cande and Kent (1992). Uncertainty envelope based on U-Pb age model or astronomically tuned age uncertainty, and the uncertainty on the width of individual chrons in the Cande and Kent (1992) profile, propagated using Equations S7–S9 (see footnote 1). For each age model, the durations of individual chrons are listed for comparison.

the late Eocene–early Oligocene to better than ~±100–150 k.y.

ACKNOWLEDGEMENTS

This work was funded through the European Community's Seventh Framework Programme (FP7/2007-2013) under grant agreement no. [215458]. The authors thank Brent Breithaupt (Bureau of Land Management, Cheyenne, Wyoming), Carla Loop, and Barbara Beasley (Nebraska National Forest, U.S. Forest Service) for providing permits to collect samples at Flagstaff Rim and TGP, Bill Lukens for help during field work, and the staff of the Fort Hoofddijk Paleomagnetic Laboratory for access to their facilities and assistance with paleomagnetic measurements. The authors thank Courtney Sprain and an anonymous reviewer for their constructive comments.

REFERENCES CITED

Beddow, H.M., Liebrand, D., Wilson, D.S., Hilgen, F.J., Sluijs, A., Wade, B.S., and Lourens, L.J., 2018, Astronomical tunings of the Oligocene-Miocene transition from Pacific Ocean Site U1334 and implications for the carbon cycle: Climate of the Past, v. 14, no. 3, p. 255–270, https://doi.org/10.5194/cp-14-255-2018.

Berggren, W.A., Kent, D.V., Flynn, J.J., and Vancouvering, J.A., 1985, Cenozoic Geochronology: Geological Society of America Bulletin, v. 96, no. 11, p. 1407–1418, https://doi.org/10.1130/0016-7606(1985)96<1407:CG>2.0.CO;2.

Besse, J., and Courtillot, V., 2002, Apparent and true polar wander and the geometry of the geomagnetic field over the last 200 Myr: Journal of Geophysical Research, v. 107, no. B11, 2300, https://doi.org/10.1029/2000JB000050.

Boardman, G.S., and Secord, R., 2013, Stable isotope paleoecology of White River ungulates during the Eocene-Oligocene climate transition in northwestern Nebraska: Palaeogeography, Palaeoclimatology, Palaeoecology, v. 375, p. 38–49, https://doi.org/10.1016/j.palaeo.2013.02.010.

Boulila, S., Vahlenkamp, M., De Vleeschouwer, D., Laskar, J., Yamamoto, Y., Palike, H., Turner, S.K., Sexton, P.F., Westerhold, T., and Rohl, U., 2018, Towards a robust and consistent middle Eocene astronomical timescale: Earth and Planetary Science Letters, v. 486, p. 94–107, https://doi.org/10.1016/j.epsl.2018.01.003.

Bronk Ramsey, C., 2008, Deposition models for chronological records: Quaternary Science Reviews, v. 27, p. 42–60, https://doi.org/10.1016/j.quascirev.2007.01.019.

Cande, S.C., and Kent, D.V., 1992, A new geomagnetic polarity time scale for the Late Cretaceous and Cenozoic: Journal of Geophysical Research. Solid Earth, v. 97, no. B10, p. 13,917–13,951, https://doi.org/10.1029/92JB01202.

Cande, S.C., and Kent, D.V., 1995, Revised calibration of the geomagnetic polarity timescale for the Late Cretaceous and Cenozoic: Journal of Geophysical Research, v. 100, no. B4, p. 6093–6095, https://doi.org/10.1029/94JB03098.

Clark, J., 1975, Controls of sedimentation and provenance of sediments in the Oligocene of the central Rocky Mountains, *in* Curtis, B.F., ed., Cenozoic history of the southern Rocky Mountains: Geological Society of America Memoir 144, p. 97–117, https://doi.org/10.1130/MEM144-p95.

Clement, B.M., 2004, Dependence of the duration of geomagnetic polarity reversals on site latitude: Nature, v. 428, no. 6983, p. 637–640, https://doi.org/10.1038/nature02459.

Coccioni, R., Marsili, A., Montanari, A., Bellanca, A., Neri, R., Bice, D.M., Brinkhuis, H., Church, N., Macalady, A., McDaniel, A., Deino, A., Lirer, F., Sprovieri, M., Maiorano, P., Monechi, S., Nini, C., Nocchi, M., Pross, J., Rochette, P., Sagnotti, L., Tateo, F., Touchard, Y., Van Simaeys, S., and Williams, G.L., 2008, Integrated stratigraphy of the Oligocene pelagic sequence in the Umbria-Marche basin (northeastern Apennines, Italy): A potential Global Stratotype Section and Point (GSSP) for the Rupelian/Chattian boundary: Geological Society of America Bulletin, v. 120, no. 3-4, p. 487–511, https://doi.org/10.1130/B25988.1.

Condon, D.J., Schoene, B., McLean, N.M., Bowring, S.A., and Parrish, R.R., 2015, Metrology and traceability of U-Pb isotope dilution geochronology (EARTHTIME Tracer Calibration Part I): Geochimica et Cosmochimica Acta, v. 164, p. 464–480, https://doi.org/10.1016/j.gca.2015.05.026.

Coxall, H.K., Wilson, P.A., Palike, H., Lear, C.H., and Backman, J., 2005, Rapid stepwise onset of Antarctic glaciation and deeper calcite compensation in the Pacific Ocean: Nature, v. 433, no. 7021, p. 53–57, https://doi.org/10.1038/nature03135.

Dinares-Turell, J., Westerhold, T., Pujalte, V., Rohl, U., and Kroon, D., 2014, Settling the Danian Astronomical Time Scale: A Prospective Global Unit Stratotype at Zumaia: Basque Basin: Strati, v. 2013, p. 191–195, https://doi.org/10.1007/978-3-319-04364-7_38.

Emry, R.J., 1973, Stratigraphy and Preliminary Biostratigraphy of the Flagstaff Rim Area, Natrona County, Wyoming: Smithsonian Contributions to Paleobiology, v. 18, p. 48, https://doi.org/10.5479/si.00810266.18.1.

Emry, R. J., 1992, Mammalian range zones in the Chadronian White River Formation at Flagstaff Rim, Wyoming: Princeton Series in Geology and Paleontology; Eocene-Oligocene climatic and biotic evolution, p. 106–115, https://doi.org/10.1515/9781400862924.106.

Emry, R.J., Russell, L.S., and Bjork, P.R., 1987, The Chadronian, Orellan, and Whitneyan North American land mammal ages, *in* Woodburne, M.O., ed., Cenozoic Mammals of North America: Geochronology and Biostratigraphy, University of California Press, p. 118–152, ISBN: 9780520053922.

Evanoff, E., Prothero, D.R., and Lander, R.H., 1992, Eocene-Oligocene climatic change in North America: The White River formation near Douglas, east-central Wyoming, *in* Prothero, D.R., and Berggren, V.A., eds., Eocene-Oligocene climatic and biotic evolution: Princeton, Princeton University Press, p. 116–130, https://doi.org/10.1515/9781400862924.116.

Evernden, J.F., Savage, D.E., Curtis, G.H., and James, G.T., 1964, Potassium-Argon dates and the Cenozoic mammalian chronology of North America: American Journal of Science, v. 262, p. 145–198, https://doi.org/10.2475/ajs.262.2.145.

Fisher, R.A., 1953, Dispersion on a sphere: Proceedings of the Royal Society of London. Series A, Mathematical and Physical Sciences, v. 217, p. 295–305, https://doi.org/10.1098/rspa.1953.0064.

Hilgen, F.J., Hinnov, L.A., Abdul Aziz, H., Abels, H.A., Batenburg, S., Bosmans, J.H.C., de Boer, B., Hüsing, S.K., Kuiper, K.F., Lourens, L.J., Rivera, T., Tuenter, E., Van de Wal, R.S.W., Wotzlaw, J.-F., and Zeeden, C., 2015, Stratigraphic continuity and fragmentary sedimentation: the success of cyclostratigraphy as part of integrated stratigraphy, *in* Smith, D.G., et al., Strata and Time: Probing the Gaps in Our Understanding: Geological Society of London Special Publication 404, p. 157–197, https://doi.org/10.1144/SP404.12.

Hilgen, F.J., Kuiper, K.F., and Lourens, L.J., 2010, Evaluation of the astronomical time scale for the Paleocene and earliest Eocene: Earth and Planetary Science Letters, v. 300, no. 1-2, p. 139–151, https://doi.org/10.1016/j.epsl.2010.09.044.

Hinnov, L.A., and Ogg, J.G., 2007, Cyclostratigraphy and the astronomical time scale: Stratigraphy, v. 4, no. 2-3, p. 239–251.

Hüsing, S.K., Hilgen, F.J., Aziz, H.A., and Krijgsman, W., 2007, Completing the Neogene geological time scale between 8.5 and 12.5 Ma: Earth and Planetary Science Letters, v. 253, no. 3-4, p. 340–358, https://doi.org/10.1016/j.epsl.2006.10.036.

Hüsing, S.K., Kuiper, K.F., Link, W., Hilgen, F.J., and Krijgsman, W., 2009, The upper Tortonian–lower Messinian at Monte dei Corvi (Northern Apennines, Italy): Completing a Mediterranean reference section for the Tortonian Stage: Earth and Planetary Science Letters, v. 282, p. 140–157, https://doi.org/10.1016/j.epsl.2009.03.010.

Hyland, E., Murphy, B., Varela, P., Marks, K., Colwell, L., Tori, F., Monechi, S., Cleaveland, L., Brinkhuis, H., van Mourik, C.A., Coccioni, R., Bice, D., and Montanari, A., 2009, Integrated stratigraphic and astrochronologic calibration of the Eocene-Oligocene transition in the Monte Cagnero section (northeastern Apennines, Italy): A potential parastratotype for the Massignano global stratotype section and point (GSSP), *in* Koeberl, C., and Montanarieds, A., eds., Late Eocene Earth—Hothouse Icehouse and Impacts: Geological Society of America Special Paper 452, p. 303–322, https://doi.org/10.1130/2009.2452(19).

Ivany, L.C., Van Simaeys, S., Domack, E.W., and Samson, S.D., 2006, Evidence for an earliest Oligocene ice sheet on the Antarctic Peninsula: Geology, v. 34, no. 5, p. 377–380, https://doi.org/10.1130/G22383.1.

Jaffey, A.H., Flynn, K.F., Glendenin, L.E., Bentley, W.C., and Essling, A.M., 1971, Precision Measurement of Half-Lives and Specific Activities of U-235 and U-238: Physical Review C: Nuclear Physics, v. 4, no. 5, p. 1889–1906, https://doi.org/10.1103/PhysRevC.4.1889.

Jovane, L., Florindo, F., Sprovieri, M., and Palike, H., 2006, Astronomic calibration of the late Eocene/early Oligocene Massignano section (central Italy): Geochemistry Geophysics Geosystems, v. 7, https://doi.org/10.1029/2005GC001195.

Jovane, L., Savian, J.F., Coccioni, R., Frontalini, F., Bancalà, G., Catanzariti, R., Luciani, V., Bohaty, S.M., Wilson, P.A., and Florindo, F., 2013, Integrated magnetobiostratigraphy of the middle Eocene–lower Oligocene interval from the Monte Cagnero section, central Italy, *in* Jovane, L., et al., eds., Magnetic Methods and the Timing of Geological Processes: Geological Society of London Special Publication 373, p. 79–95, https://doi.org/10.1144/SP373.13.

Kirschvink, J. L., 1980, The least-squares line and plane and the analysis of paleomagnetic data: examples from Siberia and Morocco: Geophysical Journal of the Royal Astronomical Society, no. 62, p. 699–718, https://doi.org/10.1111/j.1365-246X.1980.tb02601.x.

Krijgsman, W., Hilgen, F.J., Raffi, I., Sierro, F.J., and Wilson, D.S., 1999, Chronology, causes and progression of the Messinian salinity crisis: Nature, v. 400, p. 652, https://doi.org/10.1038/23231.

Kuiper, K.F., Deino, A., Hilgen, F.J., Krijgsman, W., Renne, P.R., and Wijbrans, J.R., 2008, Synchronizing rock clocks of Earth history: Science, v. 320, no. 5875, p. 500–504, https://doi.org/10.1126/science.1154339.

LaGarry, H.E., 1998, Lithostratigraphic revision and redescription of the Brule Formation (White River Group) of northwestern Nebraska, *in* Terry, D.O., LaGarry, H.E., and Hunt, R.M., eds., Depositional Environments, Lithostratigraphy and Biostratigraphy of the White River and Arikaree Groups (Late Eocene to Early Miocene, North America): Geological Society of America Special Paper 325, p. 63–91, https://doi.org/10.1130/0-8137-2325-6.63.

Larson, E.E., and Evanoff, E., 1998, Tephrostratigraphy and source of the tuffs of the White River sequence, *in* Terry, D.O., LaGarry, H.E., and Hunt, R.M., eds., Depositional Environments, Lithostratigraphy, and Biostratigraphy of the White River and Arikaree Groups (Late Eocene to Early Miocene, North America): Geological Society of America Special Paper, p. 1–14, https://doi.org/10.1130/0-8137-2325-6.1.

Laskar, J., Robutel, P., Joutel, F., Gastineau, M., Correia, A.C.M., and Levrard, B., 2004, A long-term numerical solution for the insolation quantities of the Earth: Astronomy & Astrophysics, v. 428, no. 1, p. 261–285, https://doi.org/10.1051/0004-6361:20041335.

Laskar, J., Fienga, A., Gastineau, M., and Manche, H., 2011, La2010: a new orbital solution for the long-term motion of the Earth: Astronomy and Astrophysics, v. 532, p. A89, https://doi.org/10.1051/0004-6361/201116836.

Lowrie, W., and Lanci, L., 1994, Magnetostratigraphy of the Eocene-Oligocene boundary sections in Italy—no evidence for short subchrons within 12r and 13r: Earth and Planetary Science Letters, v. 126, no. 4, p. 247–258, https://doi.org/10.1016/0012-821X(94)90110-4.

McLean, N.M., Condon, D.J., Schoene, B., and Bowring, S.A., 2015, Evaluating uncertainties in the calibration of isotopic reference materials and multi-element isotopic tracers (EARTHTIME Tracer Calibration Part II): Geochimica et Cosmochimica Acta, v. 164, p. 481–501, https://doi.org/10.1016/j.gca.2015.02.040.

Merico, A., Tyrrell, T., and Wilson, P.A., 2008, Eocene/Oligocene ocean de-acidification linked to Antarctic glaciation by sea-level fall: Nature, v. 452, no. 7190, p. 979–982, https://doi.org/10.1038/nature06853.

Meyers, S.R., 2015, The evaluation of eccentricity-related amplitude modulation and bundling in paleoclimate data: An inverse approach for astrochronologic testing and time scale optimization: Paleoceanography, v. 30, no. 12, p. 1625–1640, https://doi.org/10.1002/2015PA002850.

Mullender, T.A.T., Vanvelzen, A.J., and Dekkers, M.J., 1993, Continuous Drift Correction and Separate Identification of Ferrimagnetic and Paramagnetic Contributions in Thermomagnetic Runs: Geophysical Journal International, v. 114, no. 3, p. 663–672, https://doi.org/10.1111/j.1365-246X.1993.tb06995.x.

Obradovich, J. D., Evanoff, E., and Larson, E. E., 1995, Revised single crystal laser fusion $^{40}Ar/^{39}Ar$ ages of Chadronian tuffs in the White River Formation of Wyoming: Geological Society of America Abstract with Programs, v. 27, no. 3, p. A77.

Ogg, J.G., and Smith, A.G., 2004, The geomagnetic polarity time scale, *in* Gradstein, F.M., Ogg, J. G., and Smith, A.G., eds., A Geologic Time Scale 2004, Cambridge University Press, p. 63–86, https://doi.org/10.1017/CBO9780511536045.006.

Pälike, H., Shackleton, N.J., and Röhl, U., 2001, Astronomical forcing in Late Eocene marine sediments: Earth and Planetary Science Letters, v. 193, no. 3-4, p. 589–602. https://doi.org/10.1016/S0012-821X(01)00501-5.

Pälike, H., Norris, R.D., Herrle, J.O., Wilson, P.A., Coxall, H.K., Lear, C.H., Shackleton, N.J., Tripati, A.K., and Wade, B.S., 2006, The heartbeat of the Oligocene climate system: Science, v. 314, no. 5807, p. 1894–1898, https://doi.org/10.1126/science.1133822.

Parés, J.M., and Van der Voo, R., 2013, Non-antipodal directions in magnetostratigraphy: an overprint bias?: Geophysical Journal International, v. 192, no. 1, p. 75–81, https://doi.org/10.1093/gji/ggs027.

Prothero, D.R., 1985, Chadronian (Early Oligocene) magnetostratigraphy of eastern Wyoming—Implications for the age of the Eocene-Oligocene boundary: The Journal of Geology, v. 93, no. 5, p. 555–565, https://doi.org/10.1086/628980.

Prothero, D.R., 1996, Magnetostratigraphy of the White River Group in the High Plains, *in* Prothero, D.R., and Emry, R.J., eds., The Terrestrial Eocene-Oligocene Transition in North America: Cambridge, Cambridge University Press, p. 262–277, https://doi.org/10.1017/CBO9780511665431.014.

Prothero, D.R., and Swisher, C.C., 1992, Magnetostratigraphy and geochronology of the terrestrial Eocene-Oligocene transition in North America, *in* Prothero, D.R., and Berggren, V.A., eds., Eocene-Oligocene climatic and biotic evolution, Princeton University Press, p. 49–73, https://doi.org/10.1515/9781400862924.46.

Prothero, D.R., and Whittlesey, K.E., 1998, Magnetostratigraphy and biostratigraphy of the Orellan and Whitneyan land mammal "ages" in the White River Group, *in* Terry, D.O., LaGarry, H.E., and Hunt, R.M., eds., Depositional Environments, Lithostratigraphy and Biostratigraphy of the White River and Arikaree Groups (Late Eocene to Early Miocene, North America), Volume 325, p. 39–62, https://doi.org/10.1130/0-8137-2325-6.39.

Prothero, D.R., Denham, C.R., and Farmer, H.G., 1982, Oligocene calibration of the magnetic polarity time scale: Geology, v. 10, no. 12, p. 650–653, https://doi.org/10.1130/0091-7613(1982)10<650:OCOTMP>2.0.CO;2.

Prothero, D.R., Denham, C.R., and Farmer, H.G., 1983, Magnetostratigraphy of the White River Group and its implications for Oligocene geochronology: Palaeogeography, Palaeoclimatology, Palaeoecology, v. 42, no. 1-2, p. 151–166, https://doi.org/10.1016/0031-0182(83)90042-1.

Sahy, D., Condon, D.J., Terry, D.O., Fischer, A.U., and Kuiper, K.F., 2015, Synchronizing terrestrial and marine records of environmental change across the Eocene-Oligocene transition: Earth and Planetary Science Letters, v. 427, p. 171–182, https://doi.org/10.1016/j.epsl.2015.06.057.

Sahy, D., Condon, D.J., Hilgen, F.J., and Kuiper, K.F., 2017, Reducing disparity in radio-isotopic and astrochronology-based time scales of the Late Eocene and Oligocene: Paleoceanography, v. 32, no. 10, p. 1018–1035, https://doi.org/10.1002/2017PA003197.

Schoene, B., Condon, D.J., Morgan, L., and McLean, N., 2013, Precision and Accuracy in Geochronology: Elements, v. 9, no. 1, p. 19–24, https://doi.org/10.2113/gselements.9.1.19.

Shackleton, N.J., and Kennett, P., 1975, Paleotemperature history of the Cenozoic and the initiation of Antarctic glaciation: oxygen and carbon analyses in DSDP Sites 277, 279, and 281: Deep Sea Drilling Project Initial Reports, v. 29, p. 743–755, https://doi.org/10.2973/dsdp.proc.29.117.1975.

Stanley, K.O., and Benson, L.V., 1979, Early diagenesis of High Plains Tertiary vitric and arkosic sandstone, Wyoming and Nebraska, *in* Scholle, P.A., and Schluger, P.R., eds., Aspects of diagenesis: Society of Economic Geologists and Paleontologists Special Publication 26, p. 401–423, https://doi.org/10.2110/pec.79.26.0401.

Swisher, C.C., and Prothero, D.R., 1990, Single-crystal $^{40}Ar/^{39}Ar$ dating of the Eocene-Oligocene transition in North America: Science, v. 249, p. 760–762, https://doi.org/10.1126/science.249.4970.760.

Tauxe, L., 2010, Essentials of Paleomagnetism: University of California Press, p. 512, ISBN: 9780520260313.

Terry, D.O., 1998, Lithostratigraphic revision and correlation of the lower part of the White River Group: South Dakota to Nebraska, *in* Terry, D.O., LaGarry, H.E., and Hunt, R.M., eds., Depositional Environments, Lithostratigraphy and Biostratigraphy of the White River and Arikaree Groups (Late Eocene to Early Miocene, North America): Geological Society

of America Special Paper 325, p. 15–37, https://doi.org/10.1130/0-8137-2325-6.15.

Terry, D.O., 2001, Paleopedology of the Chadron Formation of Northwestern Nebraska: implications for paleoclimatic change in the North American midcontinent across the Eocene-Oligocene boundary: Palaeogeography, Palaeoclimatology, Palaeoecology, v. 168, no. 1-2, p. 1–38, https://doi.org/10.1016/S0031-0182(00)00248-0.

Terry, D.O., and LaGarry, H.E., 1998, The Big Cottonwood Creek Member: A new member of the Chadron Formation in northwestern Nebraska, *in* Terry, D.O., LaGarry, H.E., and Hunt, R.M., eds., Depositional Environments, Lithostratigraphy and Biostratigraphy of the White River and Arikaree Groups (Late Eocene to Early Miocene, North America): Geological Society of America Special Paper 325, p. 117–141, https://doi.org/10.1130/0-8137-2325-6.117.

Torsvik, T.H., Muller, R.D., Van der Voo, R., Steinberger, B., and Gaina, C., 2008, Global plate motion frames: Toward a unified model: Reviews of Geophysics, v. 46, no. 3, https://doi.org/10.1029/2007RG000227.

Vandamme, D., 1994, A new method to determine paleosecular variation: Physics of the Earth and Planetary Interiors, v. 85, no. 1-2, p. 131–142, https://doi.org/10.1016/0031-9201(94)90012-4.

Vandenberghe, N., Hilgen, F.J., Speijer, R.P., Ogg, J.G., Gradstein, F.M., Hammer, O., Hollis, C.J., and Hooker, J.J., 2012, The Paleogene Period, *in* Gradstein, F.M., Ogg, J.G., Schmitz, M.D., and Ogg, G.M., eds., The Geologic Time Scale 2012: Boston, Elsevier, p. 855–921, https://doi.org/10.1016/B978-0-444-59425-9.00028-7.

Westerhold, T., and Röhl, U., 2009, High resolution cyclostratigraphy of the early Eocene - new insights into the origin of the Cenozoic cooling trend: Climate of the Past, v. 5, no. 3, p. 309–327, https://doi.org/10.5194/cp-5-309-2009.

Westerhold, T., Rohl, U., Laskar, J., Raffi, I., Bowles, J., Lourens, L.J., and Zachos, J.C., 2007, On the duration of magnetochrons C24r and C25n and the timing of early Eocene global warming events: Implications from the Ocean Drilling Program Leg 208 Walvis Ridge depth transect: Paleoceanography, v. 22, no. 1, 10.1029/2006PA001322.

Westerhold, T., Rohl, U., Raffi, I., Fornaciari, E., Monechi, S., Reale, V., Bowles, J., and Evans, H.F., 2008, Astronomical calibration of the Paleocene time: Palaeogeography, Palaeoclimatology, Palaeoecology, v. 257, no. 4, p. 377–403, https://doi.org/10.1016/j.palaeo.2007.09.016.

Westerhold, T., Rohl, U., Donner, B., McCarren, H.K., and Zachos, J.C., 2011, A complete high-resolution Paleocene benthic stable isotope record for the central Pacific (ODP Site 1209): Paleoceanography, v. 26, https://doi.org/10.1029/2010PA002092.

Westerhold, T., Röhl, U., Wilkens, R., Pälike, H., Lyle, M., Jones, T.D., Bown, P., Moore, T., Kamikuri, S., Acton, G., Ohneiser, C., Yamamoto, Y., Richter, C., Fitch, P., Scher, H., and Liebrand, D., and the Expedition 320/321 Scientists, 2012, "Revised composite depth scales and integration of IODP Sites U1331–U1334 and ODP Sites 1218–1220," *in* Pälike, H., Lyle, M., Nishi, H., Raffi, I., Gamage, K., Klaus, A., and the Expedition 320/321 Scientists, eds., Proceedings, IODP, 320/321: Tokyo, Integrated Ocean Drilling Program Management International, Inc., https://doi.org/10.2204/iodp.proc.320321.201.2012.

Westerhold, T., Rohl, U., Palike, H., Wilkens, R., Wilson, P.A., and Acton, G., 2014, Orbitally tuned timescale and astronomical forcing in the middle Eocene to early Oligocene: Climate of the Past, v. 10, no. 3, p. 955–973, https://doi.org/10.5194/cp-10-955-2014.

Westerhold, T., Roehl, U., Frederichs, T., Bohaty, S.M., and Zachos, J.C., 2015, Astronomical calibration of the geol*ogical timescale: closing the middle Eocene gap: Climate of the Past, v. 11, no. 9, p. 1181–1195, https://doi.org/10.5194/cp-11-1181-2015.

Wilson, D.S., 1993, Confirmation of the astronomical calibration of the magnetic polarity timescale from seafloor spreading rates: Nature, v. 364, p. 788, https://doi.org/10.1038/364788a0.

Wotzlaw, J.F., Hüsing, S.K., Hilgen, F.J., and Schaltegger, U., 2014, High-precision zircon U-Pb geochronology of astronomically dated volcanic ash beds from the Mediterranean Miocene: Earth and Planetary Science Letters, v. 407, p. 19–34, https://doi.org/10.1016/j.epsl.2014.09.025.

Zachos, J., Pagani, M., Sloan, L., Thomas, E., and Billups, K., 2001, Trends, rhythms, and aberrations in global climate 65 Ma to present: Science, v. 292, no. 5517, p. 686–693, https://doi.org/10.1126/science.1059412.

Zanazzi, A., Kohn, M.J., MacFadden, B.J., and Terry, D.O., 2007, Large temperature drop across the Eocene-Oligocene transition in central North America: Nature, v. 445, no. 7128, p. 639–642, https://doi.org/10.1038/nature05551.

Zanazzi, A., Kohn, M.J., and Terry, D.O., 2009, Biostratigraphy and paleoclimatology of the Eocene-Oligocene boundary section at Toadstool Park, northwestern Nebraska, USA, *in* Koeberl, C., and Montanarieds, A., eds., Late Eocene Earth—Hothouse Icehouse and Impacts: Geological Society of America Special Paper 452, p. 197–214, https://doi.org/10.1130/2009.2452(13).

Zijderveld, J.D.A., 1967, A.C. demagnetization of rocks: analysis of results, *in* Collinson, D.W., Creer, K.M., and Runcorn, S.K., eds., Methods in Paleomagnetism: Elsevier, p. 254–286, ISBN: 9781483274997.

Science Editor: Bradley S. Singer
Associate Editor: Michael Smith

Manuscript Received 16 November 2018
Revised Manuscript Received 28 February 2019
Manuscript Accepted 9 April 2019

Printed in the USA